AGU PUBLICATIONS

JGR

Journal of Geophysical Research: Solid Earth

RESEARCH ARTICLE
10.1002/2017JB014378

Key Points:
- The lower parts of the forearc basin sequences (<8.5-3.0 Ma) are found in the Lichi Mélange
- Arcward back thrusting occurring no later than ~3.4 Ma deformed and uplifted the lower forearc sequences
- The oldest forearc sediments in the Lichi Mélange register the onset of the Taiwan arc-continent collision within <8.5-6.4 Ma

Supporting Information:
- Supporting Information S1
- Table S1
- Table S2

Correspondence to:
C.-Y. Huang and Y. Yan,
huangcy@mail.ncku.edu.tw;
yanyi@gig.ac.cn

Citation:
Chen, W.-H., C.-Y. Huang, Y. Yan, Y. Dilek, D. Chen, M.-H. Wang, X. Zhang, Q. Lan, and M. Yu (2017), Stratigraphy and provenance of forearc sequences in the Lichi Mélange, Coastal Range: Geological records of the active Taiwan arc-continent collision, *J. Geophys. Res. Solid Earth*, *122*, 7408–7436, doi:10.1002/2017JB014378.

Received 27 APR 2017
Accepted 22 AUG 2017
Accepted article online 28 AUG 2017
Published online 18 SEP 2017

©2017. American Geophysical Union. All Rights Reserved.

Stratigraphy and provenance of forearc sequences in the Lichi Mélange, Coastal Range: Geological records of the active Taiwan arc-continent collision

Wen-Huang Chen[1], Chi-Yue Huang[1,2,3], Yi Yan[1], Yildirim Dilek[4], Duofu Chen[1,5], Ming-Huei Wang[6], Xinchang Zhang[1], Qing Lan[7], and Mengming Yu[1]

[1]Key Laboratory of Ocean and Marginal Sea Geology, Guangzhou Institute of Geochemistry, Chinese Academy of Sciences, Guangzhou, China, [2]School of Ocean and Earth Science, Tongji University, Shanghai, China, [3]Department of Earth Sciences, National Cheng Kung University, Tainan, Taiwan, [4]Department of Geology and Environmental Earth Science, Miami University, Oxford, Ohio, USA, [5]Shanghai Engineering Research Center of Hadal Science and Technology, College of Marine Sciences, Shanghai Ocean University, Shanghai, China, [6]Exploration and Development Research Institute, CPC Corporation, Taiwan, Miaoli, Taiwan, [7]State Key Laboratory of Ore Deposit Geochemistry, Institute of Geochemistry, Chinese Academy of Sciences, Guiyang, China

Abstract The Lichi Mélange in the Coastal Range, eastern Taiwan, is considered as sheared forearc sequences. However, the age of these sequences is still uncertain, and their significance for the arc-continent collision has been overlooked. Based on field surveys and micropaleontological analysis, four independent biostratigraphic units ranging from <8.5 to 3.0 Ma are discerned in the Lichi Mélange. These units are obviously older than the remnant forearc sequences in the east (3.4–1.2 Ma), supporting the interpretation that the Lichi Mélange arose from the shearing of the lower forearc basin sequences. The stratigraphy also suggests that the older forearc strata (<8.5–3.4 Ma) were deformed and uplifted as a bathymetric high similar to the Huatung Ridge in the western North Luzon Trough by arcward back thrusting before 3.4 Ma, while sedimentation continued in the remnant forearc basin in the east during 3.4–1.2 Ma. The older forearc strata possess vitrinite reflectance values even lower than those of the remnant forearc sequences, which also supports that they were uplifted by back thrusting and therefore did not experience significant burial. Neodymium isotope analysis shows that the <8.5–6.4 Ma forearc sediments were sourced from both the volcanic arc and the accretionary prism, indicating the emergence of the accretionary prism within <8.5–6.4 Ma. It might have resulted from the underplating of thinned continental crust and provides a good time constraint for the onset of arc-continent collision. The post 6.4 Ma forearc sediments were mainly derived from the accretionary prism, reflecting its constant uplift and large-scale exposure.

1. Introduction

Forearc basins preserve tectonic, erosional, and magmatic records in convergent margins, and thus, they are important for understanding subduction-collision histories [*Dickinson*, 1995; *Orme et al.*, 2015]. During the subduction and subsequent collision periods, forearc basins often undergo active plate boundary deformations [*Cavazza and Barone*, 2010; *Kelsey et al.*, 2012], which further affect their sedimentation [*Huang et al.*, 2008; *Paquet et al.*, 2011; *Williams and Graham*, 2013]. Sediments shed from the adjacent volcanic arcs are often trapped in the forearc basins and thus provide excellent records of magmatic evolution [e.g., *Linn et al.*, 1991; *Kimbrough et al.*, 2001]. Once the accretionary prisms are uplifted and subaerially exposed, they also contribute sediments to the forearc basins [*Dickinson*, 1995]. However, this process has been documented in only a few forearc basins, such as the Great Valley forearc basin in California [*Mitchell et al.*, 2010] and the Coastal Range forearc basin in eastern Taiwan [*Dorsey and Lundberg*, 1988; *Teng*, 1990; *Huang et al.*, 2006]. The study of modern forearc basins relies upon seismic surveys and boreholes, which are unfortunately limited because forearc basins usually lack petroleum resources. Outcrops of ancient forearc basins provide good opportunities to investigate their sedimentary records, but most of these basins have been badly damaged by complex collisional tectonism [*Dickinson*, 1995; *Williams and Graham*, 2013]. Taiwan is one of the youngest collisional orogens and has undergone the least complicated deformation relative to ancient collisional orogens [*Huang et al.*, 2000, 2006; *Clift et al.*, 2003], which largely facilitates the study of sedimentary records in the forearc basin.

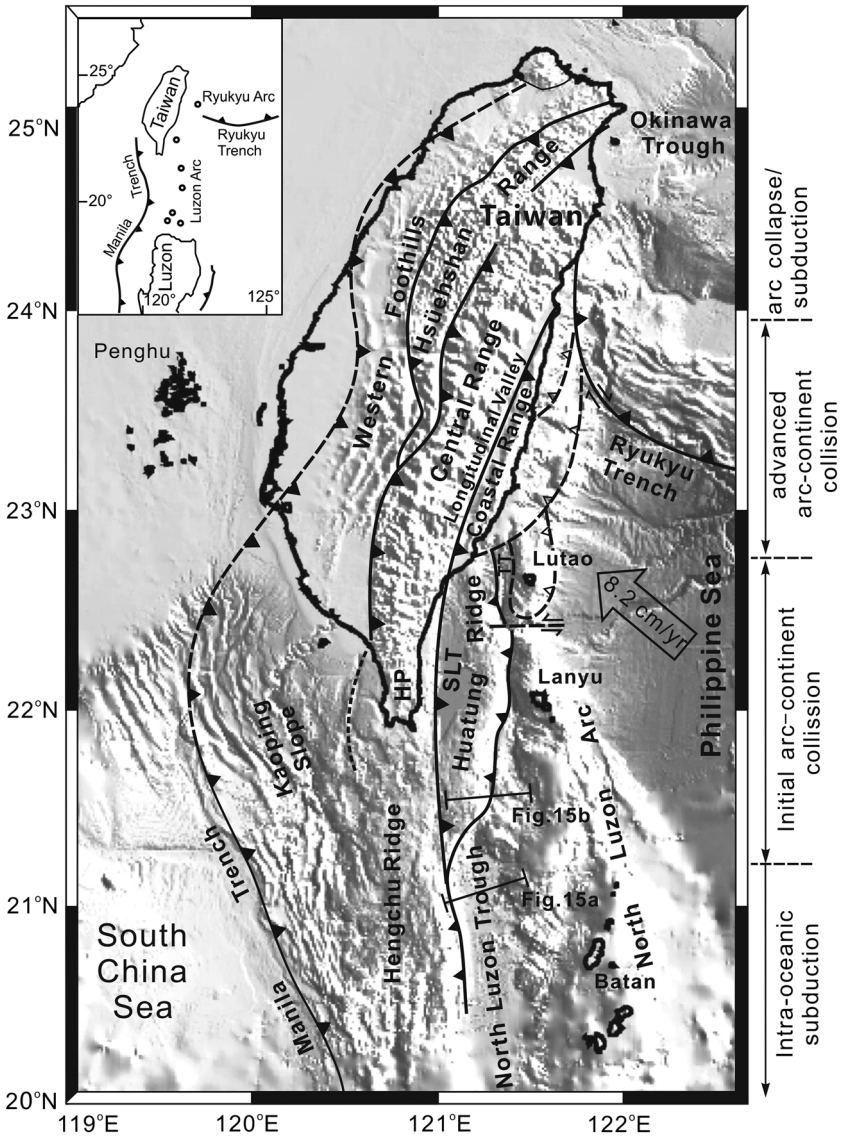

Figure 1. Shaded relief map and tectonic setting of the Taiwan region showing four tectonic processes operating from south to north (modified from *Huang et al.*, 2008). HP = Hengchun Peninsula, SLT = Southern Longitudinal Trough, and TT = Taitung Trough.

Offshore and on land Taiwan, different stages from oceanic subduction to arc-continent collision are operating simultaneously along the convergent boundary (Figure 1). Numerous marine geological surveys have revealed that the North Luzon Trough forearc basin in the initial arc-continent collision zone has been destroyed and semiclosed and that arcward back thrusting has deformed and uplifted the forearc strata as the Huatung Ridge [*Reed et al.*, 1992; *Lundberg et al.*, 1997; *Chang et al.*, 2001; *Huang et al.*, 2008; *Hirtzel et al.*, 2009]. In the advanced arc-continent collision zone, several remnants of the forearc basin (remnant forearc basins), which are filled with young (Pliocene-Pleistocene) syncollisional sediments without significant deformation, are preserved on the Coastal Range [*Huang et al.*, 1995] (Figure 2). Juxtaposed against the remnant forearc basins, the Lichi Mélange in the southwestern Coastal Range was once considered as a sedimentary olistostrome slumped from the Central Range accretionary prism in the western part of the forearc basin [*Wang*, 1976; *Page and Suppe*, 1981; *Barrier and Muller*, 1984]. However, intensive marine surveys off southern Taiwan and field surveys on land Coastal Range since early 1990s support the idea that the Lichi Mélange is the northern extension of the Huatung Ridge and arose from the shearing of lower forearc sequences [*Chang et al.*, 2000, 2001; *Huang et al.*, 2000, 2008; *Chi et al.*, 2014]. The true sedimentary age is difficult to constrain due to the disruption of stratal continuity. Previous biostratigraphic studies on the

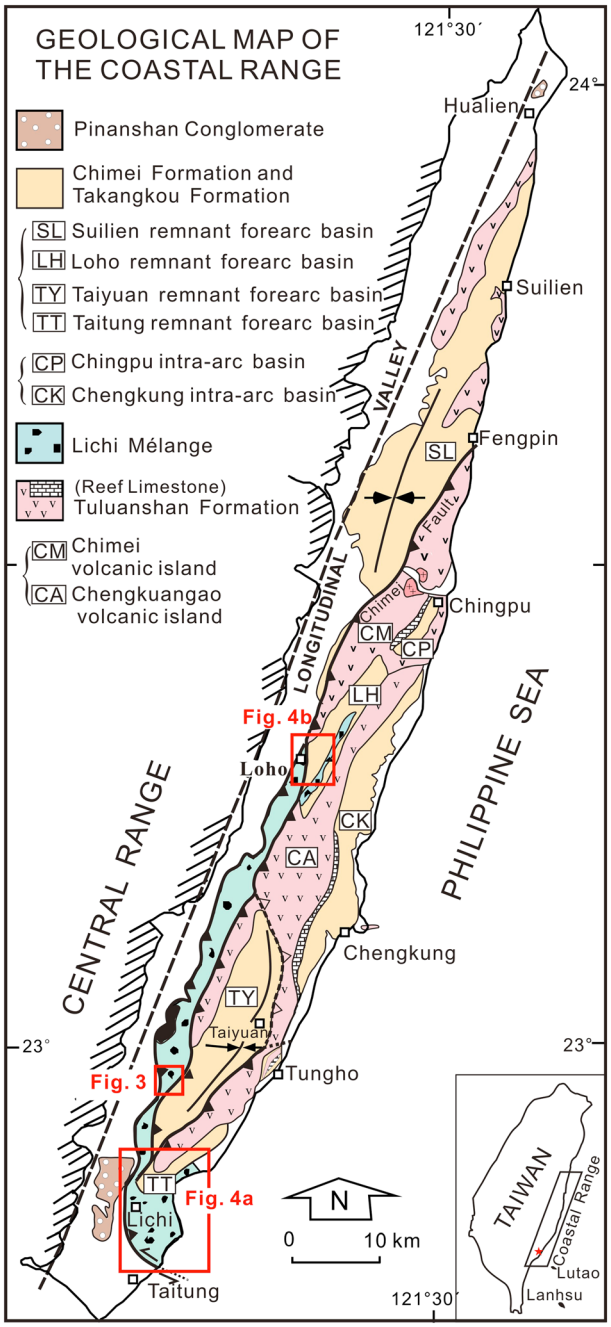

Figure 2. Geological map of the Coastal Range (adapted from *Hsu* [1956, 1976] and *Huang et al.* [2006]). The Coastal Range is composed of two volcanic islands associated with two intra-arc basins, four remnant forearc basins, and the Lichi Mélange. The red rectangles mark the locations of Figures 3, 4a, and 4b.

Lichi Mélange include separate works on planktonic foraminifera and calcareous nannofossils, and these studies found a chaotic mixing of fossils indicative of Oligocene to Pliocene ages [*Chang*, 1967, 1969; *Huang*, 1969; *Chi et al.*, 1981; *Chi*, 1982]. Although notable late Miocene assemblages were reported in these studies, from the viewpoint of the olistostrome slumping model, they were considered as reworked fossils, and the sedimentary age of the Lichi Mélange was simply assigned to the Pliocene using the youngest fossils [*Page and Suppe*, 1981; *Huang*, 1969; *Chi et al.*, 1981; *Chi*, 1982]. Therefore, determining the precise age of the Lichi Mélange is vital for establishing a more complete stratigraphy of the forearc basin. This information is also helpful for understanding the temporal-spatial variation of the forearc sequences, which can be applied to investigate whether arcward back thrusting has also occurred in the Coastal Range forearc basin as well as its effects on forearc sedimentation.

The onset of the arc-continent collision has been controversial and assigned to a rather wide range of ages between 12 and 2 Ma using different kinematic models, e.g., ~12 Ma based on the paleoposition of the North Luzon Arc [*Teng*, 1990], ~6.5 Ma based on the onset of orogenic loading-related plate flexure in the western Taiwan foreland [*Lin et al.*, 2003], and ~4 Ma based on plate boundary reconstruction [*Suppe*, 1984]. A large amount of thermochronometric data on the metamorphic rocks of the Central Range have been accumulated over the years. Most of the zircon fission track data showed that cooling from above 300°C started at approximately 6–5 Ma in both the northern and southern Central Range [*Liu et al.*, 2001; *Lee et al.*, 2006, 2015], suggesting that collision was ongoing at that time. Nevertheless, some thermochronometric data indicated that the cooling of the Central Range occurred earlier than ~6 Ma, such as a biotite Ar-Ar age of 7.9 ± 0.1 Ma [*Lo and Onstott*, 1995] and a zircon fission track age of 7.1 ± 1.3 Ma [*Mesalles et al.*, 2014]. As the sedimentary records can be obtained from both the foreland basin and the forearc basin, the uplift and emergence of the Central Range accretionary prism is regarded as an effective indicator of the onset of collision [*Huang et al.*, 2000,

2006]. Dating the emergence of the accretionary prism can thus provide a first-order constraint for understanding how plate convergence is accommodated to form mountain belts. Hitherto, the study of the sedimentary record in the Coastal Range forearc basin has been limited to only the remnant forearc basins. The emergence of the accretionary prism is dated at ~5 Ma, based on the oldest remnant forearc sequences [*Dorsey and Lundberg*, 1988; *Teng*, 1990; *Huang et al.*, 2006]. However, in western Taiwan, the basal foreland surface separating the Taiwan-sourced foreland basin sequences from the continent-derived passive margin sequences below has been estimated as ~6.5 Ma in age [*Lin et al.*, 2003]. This age implies that the accretionary prism had been subaerially exposed at that time, much earlier than that recorded in the remnant forearc basin. The emergence and then subaerial exhumation of the accretionary prism are usually associated with the cooling events. The older cooling events observed in the Central Range [*Lo and Onstott*, 1995; *Mesalles et al.*, 2014] are also earlier than the emergence of the accretionary prism recorded in the remnant forearc basin. Therefore, in the forearc basin, the emergence of the accretionary prism might be recorded in the lower forearc sequences preserved in the Lichi Mélange.

The primary purposes of this study are to determine the age of the forearc sequences preserved in the Lichi Mélange, to reconstruct the forearc basin in the middle and southern Coastal Range, and to obtain the sedimentary records of arc-continent collision. Considering the difficulty of dating sediments in the mélanges, we date the Lichi Mélange using integrated biostratigraphy of both planktonic foraminifera and calcareous nannofossils with an examination of the field occurrences. Then, thermal analyses of the Lichi Mélange and the remnant forearc sequences are performed using the vitrinite reflectance technique to understand the burial history and the tectonic evolution of the forearc basin. These data are integrated with the temporal and spatial distribution of the forearc sequences to reveal how back thrusting controlled the forearc sedimentation. Lastly, we conduct provenance analysis on the Lichi Mélange and the remnant forearc sequences using Nd isotopes to elucidate the timing of the emergence of the accretionary prism.

2. Geological Setting

2.1. Regional Tectonics of Taiwan

Taiwan is located along the boundary between the Eurasian and Philippine Sea plates and at the junction between two opposite subduction systems (Figure 1). To the southwest, the oceanic lithosphere of the South China Sea, belonging to the Eurasian plate, subducts eastward beneath the Philippine Sea plate along the Manila Trench [*Tsai*, 1986]. To the northeast, the Philippine Sea plate subducts northward beneath the Eurasian plate along the Ryukyu trench. The continuous subduction of the South China Sea since ~16 Ma along the Manila Trench has developed the Hengchun Ridge accretionary prism, the North Luzon Trough forearc basin and the North Luzon Arc [*Huang et al.*, 1992, 1997]. The North Luzon Arc moves northwestward toward the Eurasian plate and obliquely collides with the Asian continental margin, leading to the emergence of Taiwan Island. Hence, marine geological units and structures off southern Taiwan extend northward to Taiwan Island.

Taiwan Island can be divided into three major geological units from west to east: the fold-and-thrust belt (the Coastal Plain-Western Foothills-Hsüehshan Range), the accretionary prism (the Central Range-Hengchun Peninsula), and the volcanic arc-forearc basin (the Coastal Range) [*Huang et al.*, 2000, 2006]. The Hengchun Peninsula-Central Range represents the northward extension of the Hengchun Ridge accretionary prism (in the following discussion, we combine them as the Taiwan accretionary prism), while the Coastal Range represents the northward extension of the North Luzon Trough forearc basin and the North Luzon Arc (Figure 1). Due to the oblique arc-continent collision, the orogeny in Taiwan propagates from north to south [*Suppe*, 1981]. Based on the geological and geophysical features between 20° and 25°N, *Huang et al.* [2000] recognized four simultaneous tectonic processes. From south to north, these processes are intraoceanic subduction, initial arc-continent collision, advanced arc-continent collision, and arc collapse/subduction (Figure 1), and they represent four stages of the tectonic evolution of Taiwan occurring sequentially since the middle Miocene [*Huang et al.*, 2000, 2006]. In the Hengchun Peninsula within the initial arc–continent collision zone, the middle to late Miocene turbidities of the accretionary prism are exposed. In contrast, the Paleozoic-Mesozoic metamorphic basement rocks, the Eocene shallow-marine metasandstones and the early to middle Miocene deep-sea slates crop out along the Central Range to the north of 22°30′ [*Chang*, 1972; *Huang et al.*, 1997].

2.2. Geology of the Coastal Range

In the advanced arc-continent collision zone from 22°40′ to 24°N, the North Luzon Arc and forearc have been thrusting westward onto the eastern Central Range along the Longitudinal Valley (the arc-prism boundary) to form the present-day Coastal Range. The lithostratigraphy of the Coastal Range is composed of four units: (1) the Miocene to early Pliocene volcanic agglomerate of the Tuluanshan Formation, (2) the Pliocene to Pleistocene coherent flysch sequences of the Takangkou and Chimei Formations, (3) the Lichi Mélange, and (4) the Pleistocene fluvial Pinanshan Conglomerate [*Hsu*, 1956, 1976] (Figure 2). Tectonostratigraphically, the Coastal Range can be divided into two independent volcanic islands (Chimei volcanic island in the north and Chengkuangao volcanic island in the south) with two intra-arc basins (Chingpu intra-arc basin in the north and Chengkuangao intra-arc basin in the south), four remnant forearc basins (from north to south: Suilien, Loho, Taiyuan, and Taitung remnant forearc basins), and the forearc collisional Lichi Mélange [*Huang et al.*, 2006, 2008] (Figure 2). The remnant forearc basins and volcanic islands are thrust westward onto the Lichi Mélange along the Tuluanshan Fault.

The ancient volcanic islands are composed mainly of andesitic volcanic rocks of the Tuluanshan Formation, including lava flows, dikes, agglomerates, volcanic breccias, tuffs, and epiclastic rocks [*Hsu*, 1956] (Figure 2). These two volcanic islands possess distinct geochemical signatures [*Chen et al.*, 1990b] and dissimilar overlying fringing reef limestones [*Huang et al.*, 1995]. The volcanism of the Chimei and Chengkuangao volcanic islands ceased at 6–5 Ma and ~3.3 Ma, respectively [*Lo et al.*, 1994; *Yang et al.*, 1995; *Huang et al.*, 2006]. Although they have been thrust westward and accreted as the Coastal Range, the majority of the volcanic islands are still preserved offshore east of the Coastal Range [*Shyu and Chen*, 1991] (Figure 1).

The remnant forearc basins are filled with deep-sea turbidites of the Takangkou and Chimei Formations [*Hsu*, 1956] (Figure 2). These two formations are referred to collectively as the "Takangkou Formation" below. The remnant forearc basins lie to the west of the volcanic ridge (Figure 2). They were parts of a continuous forearc basin separated by thrusting during the arc-continent collision and are equivalent to the modern Taitung Trough east of the Huatung Ridge (Figure 1). It was generally accepted that the Takangkou Formation is NN13–NN19 (~5.0–1.2 Ma) in age based on calcareous nannofossils [*Chi et al.*, 1981]. However, the sedimentary ages determined by calcareous nannofossils and by planktonic foraminifera [*Chang*, 1967, 1968, 1969] for a single section are usually inconsistent. For example, in the Taitung remnant forearc basin, the upstream area of Chunchieh-Chi was dated as Zones N19–N21 (5.5–1.9 Ma) based on planktonic foraminifera [*Chang*, 1967], whereas it was dated as Zone NN15 (3.9–3.7 Ma) using calcareous nannofossils [*Chi et al.*, 1981]. Moreover, the ages of the remnant forearc basins might differ from one another. Recent studies integrating these two microfossil groups showed that the Loho remnant forearc basin was deposited during 3.4–3.0 Ma, while the Taiyuan and the Taitung remnant forearc basins were deposited during 3.4–1.2 Ma [*Horng and Shea*, 1996; *Chen et al.*, 2015].

Previous provenance studies on the Coastal Range mainly focused on the remnant forearc basins using the methods of sandstone petrology, clay mineralogy, and detrital zircon thermochronology. These studies showed that the provenance of the remnant forearc basins changed from the volcanic arc to the exposed accretionary prism at the base of the Takangkou Formation [*Teng*, 1979; *Dorsey*, 1988; *Huang et al.*, 2006]. Another finding was the rapid exhumation and unroofing of the metamorphic basement of the eastern Central Range. This process was demonstrated by the presence of the medium-grade metamorphic fragments, as well as the appearance of the zircons with fission track ages reset by the Taiwan orogeny, in the remnant forearc sequences since ~2 Ma [*Dorsey*, 1988; *Kirstein et al.*, 2010]; it was also indicated by the upward increasing illite crystallinity through the remnant forearc sequences [*Dorsey et al.*, 1988]. However, in these provenance analyses, the forearc sequences preserved in the Lichi Mélange were not taken into account.

2.3. Previous Biostratigraphic Study of the Lichi Mélange

The Lichi Mélange on the southwestern flank of the Coastal Range is a distinct unit characterized by block-in-matrix fabric. This mélange consists of an intensively sheared muddy matrix intermixed with many indigenous and exotic blocks of various sizes and lithologies. The lithologies of these blocks include sedimentary rocks, andesitic rocks, and basic-ultrabasic rocks [*Hsu*, 1976; *Page and Suppe*, 1981]. The latter are also known as the East Taiwan Ophiolite [*Liou et al.*, 1977]. Most of the Lichi Mélange is located to the west of the remnant

forearc basin and crops out as a narrow belt with a length of approximately 65 km along the Longitudinal Valley. Small outcrops are also found in the center of the Loho remnant forearc basin and to the east of the Taitung remnant forearc basin (Figure 2).

Paleontologists have attempted to determine the sedimentary age of the Lichi Mélange despite the lack of stratal continuity. The earliest work was the planktonic foraminiferal study by *Chang* [1967, 1969]. He reported the presence of a late Miocene foraminiferal assemblage in the southern tip of the Coastal Range and the appearance of early Pliocene index species to the north of its type locality (Lichi village) (Figure 2). When olistostromal theorists cited this work, they arbitrarily assigned the Lichi Mélange to the Pliocene based on the youngest fossils [e.g., *Page and Suppe*, 1981]. *Huang* [1969] studied the planktonic foraminifera from the Shishan No. 1 well located at the southern tip of the Lichi Mélange (Figure 4a) and found numerous Miocene faunal assemblages. However, he dated the Lichi Mélange as Pliocene based on the occasional appearance of few Pliocene index species. Similar results have been deduced from the calcareous nannofossils studies. *Chi et al*. [1981] and *Chi* [1982] assigned the Lichi Mélange to the early Pliocene (Zones NN12–NN15), although the Miocene fossils indicative of Zones NN9–NN11 were usually recovered from the lower part of the Lichi Formation in their samples. *Barrier and Muller* [1984] considered that the Lichi Mélange is an olistostrome imbedded in the Takangkou Formation and thus constrained the Lichi Mélange within Zone NN15 based on the ages of the overlying and underlying Takangkou Formation. Most of the above researchers advocated the olistostromal origin and thus assigned the Lichi Mélange to the Pliocene in light of the youngest fossils. Consequently, they treated the Miocene fossils as the reworked fossils regardless of the field occurrence. Therefore, the discrimination of the reworked fossils is the key to dating the forearc sequences in the Lichi Mélange.

3. Sampling and Study Methods

We studied the Lichi Mélange and the remnant forearc basin using the methods of field survey, micropaleontology, vitrinite reflectance, and Nd isotopes to reconstruct the biostratigraphic framework, burial history, and provenance evolution of the forearc basin in the middle and southern Coastal Range.

Muddy matrix and mudstone samples of the Lichi Mélange were collected from three areas. The first and most important is the Mukeng-Chi section along the Mukeng-Chi and its tributaries (Figure 3). This section lies to the west of the Taiyuan remnant forearc basin. Fifty-eight samples in total were collected for planktonic foraminiferal analysis, 10 of which were selected for calcareous nannofossil analysis. Subsequently, 16 and 21 samples were chosen primarily from samples with well-constrained ages for vitrinite reflectance and Nd isotope analysis, respectively. The second area is the southern tip of the Coastal Range (Figure 4a). The Lichi Mélange in this area is located to the south and southeast of the Taitung remnant forearc basin. Thirty-seven samples were collected from north to south mainly along the Tulanpi Coast, the downstream region of the Chunchieh-Chi, the Juchiang-Chi, and the downstream area of the Peinan River. Among these samples, two were selected for calcareous nannofossil analysis, and five were selected for vitrinite reflectance analysis. The third area is the middle part of the Coastal Range (Figure 4b). In this area, the Lichi Mélange not only lies to the west of the Loho remnant forearc basin but also crops out in the basin center as a window structure. The biostratigraphy has been constrained by *Chen et al*. [2015] using planktonic foraminifera and calcareous nannofossils. Two samples were selected for vitrinite reflectance analysis.

For the Taiyuan remnant forearc basins in the east, we adopted the biostratigraphic framework established by *Horng and Shea* [1996]. For the Loho and the Taitung remnant forearc basins, the biostratigraphic frameworks established by *Chen et al*. [2015] were followed. Six mudstone samples of the Taitung remnant forearc basin were chosen for vitrinite reflectance analysis, while four samples were chosen for Nd isotope analysis (Figure 4a).

A detailed field survey of the Lichi Mélange was conducted mainly along the Mukeng-Chi section. This section was previously investigated by *Chang et al*. [2000, 2001] and *Huang et al*. [2008]. In light of the observation of the structural framework, they identified four main units (α to δ) with different degrees of deformation following the method of *Raymond* [1984]. However, they defined these units based on deformation criteria, disregarding the stratigraphic data, and even presumed that these units are laterally continuous. To enable a simpler and more objective analysis, we divided the field occurrence of the Lichi Mélange into two distinct facies: the broken formation that is deformed to different degrees but without allochthonous blocks [*Hsü*,

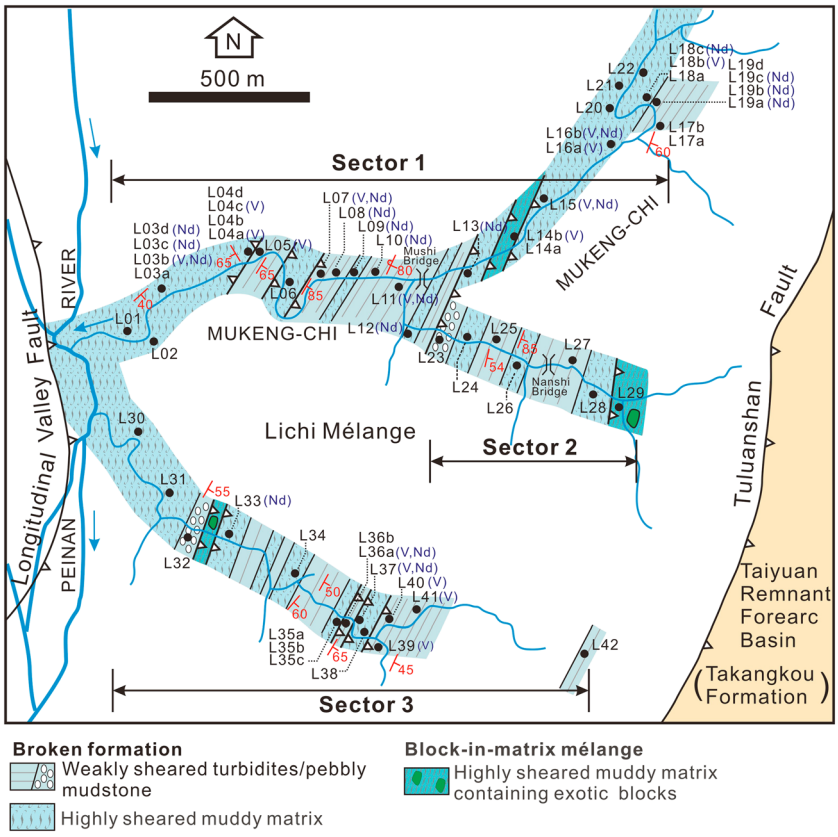

Figure 3. Geological map and sampling sites of the Lichi Mélange along the Mukeng-Chi section west of the Taiyuan remnant forearc basin. The Lichi Mélange is divided into two facies: broken formation and block-in-matrix mélange. The samples used for vitrinite reflectance and Nd isotopic analyses are marked by "V" and "Nd" in parentheses, respectively. The thrust faults inside the Lichi Mélange are based on our field observations including data of *Chang et al.* [2000] and our biostratigraphic study.

1968; *Festa et al.*, 2012] and the block-in-matrix mélange with allochthonous basic-ultrabasic blocks embedded in a highly sheared matrix [e.g., *Harris et al.*, 1998]. These two facies are shown on the geological map of the Mukeng-Chi section (Figure 3).

The biostratigraphic study of the Lichi Mélange was primarily based on planktonic foraminifera (95 samples in total) supplemented by calcareous nannofossils (12 samples in total). Planktonic foraminifera were separated from 200 g of muddy matrix/mudstone using conventional methods. Foraminiferal tests off the 100-mesh screen were picked for identification and counting under a stereomicroscope and/or scanning electron microscope (SEM). For the samples yielding abundant foraminiferal tests, at least 200 individuals were identified and counted. Standard zonations of planktonic foraminifera established from low-latitude regions by *Blow* [1969] and datum planes (FAD: first appearance datum; LAD: last appearance datum) documented by *Wade et al.* [2011] were followed (Figure 7). Five to 10 g of each sample were prepared for calcareous nannofossil analysis employing standard smear-slide techniques [*Bown and Young*, 1998]. More than 100 fields of view (FOV) for each slide were examined randomly under a polarizing microscope with 1600-fold magnification. Five classes were used to denote the floral abundances (abundant: $>$ 100 specimens/20 FOV; common: 51–100 specimens/20 FOV; few: 21–50 specimens/20 FOV; rare: 2–20 specimens/20 FOV; present: only 1 specimen/$\geq$ 20 FOV). The zonal scheme of calcareous nannofossils proposed by *Martini* [1971] and datum planes compiled by *Anthonissen and Ogg* [2012] were followed (Figure 7).

A total of 29 samples was prepared for vitrinite reflectance analysis using the method of extracting kerogen from 200 g of crushed bulk rock. The random reflectance (Ro expressed in percent) of vitrinite was measured on polished sections of concentrates of kerogen under a Carl Zeiss Axio Scope A1 Pol microscope equipped with an MSP 400 photometer. The extraction of the kerogen and the measurement of the vitrinite reflectance followed the National Standard of China GB/T 19144-2010 and SY/T 5124-2012, respectively.

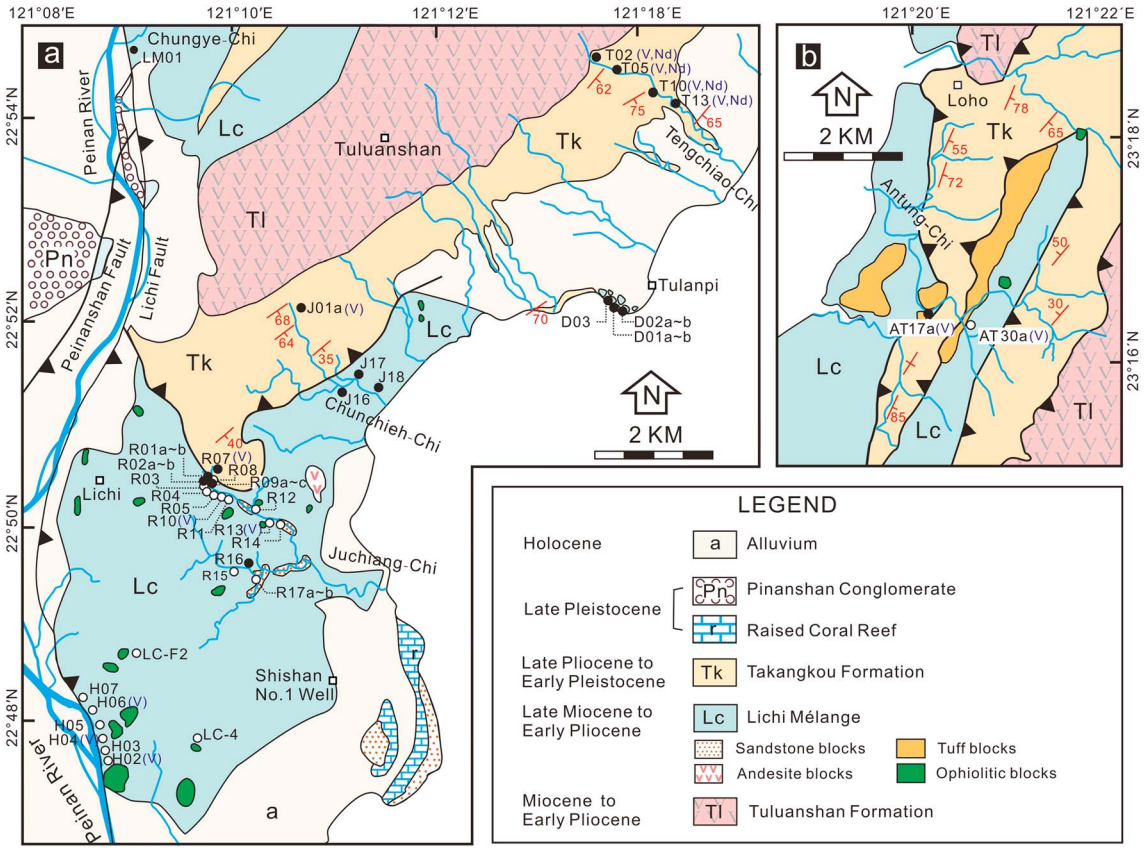

Figure 4. (a) Geological map and sampling sites of the southern end of the Coastal Range. The biostratigraphic framework of the Taitung remnant forearc basin (Takangkou Formation) follows *Chen et al.* [2015]. (b) Geological map and sampling sites of the Lichi Mélange in the middle Coastal Range. The biostratigraphic frameworks of the Lichi Mélange in this area and the Loho remnant forearc basin (Takangkou Formation) also follow *Chen et al.* [2015]. Open circles mark samples without planktonic foraminifera. The samples used for vitrinite reflectance and Nd isotopic analyses are marked by "V" and "Nd" in parentheses, respectively.

A total of 25 samples for Nd isotope analysis was crushed, powdered, and then leached with 2 N acetic acid (HAc) to remove biogenic carbonates. The solid residue was collected by centrifugation, oven dried at 100°C, and ground to powder <75 μm. The sample powders were heated at 700°C to remove organic materials and then digested in a high-pressure Teflon bomb using a HNO_3 + HF acid mixture and finally dissolved by a 2N HCl solution. The sample solution was passed through a column filled with AG50-X8 cation resin and subsequently an LN Spec (HDEHP-based) column to separate Nd from the rare earth elements. The Nd measurements were performed on a MicroMass Isoprobe multicollector inductively coupled plasma mass spectrometer (MC-ICP-MS) at the State Key Laboratory of Isotope Geochemistry at Guangzhou Institute of Geochemistry, Chinese Academy of Sciences. The measured $^{143}Nd/^{144}Nd$ ratios were normalized to $^{146}Nd/^{144}Nd = 0.7219$. A standard Nd solution, Shin Etsu JNdi-1, was repeatedly measured with the samples to monitor the quality of measurements, yielding a mean value of 0.512094 ± 4 (2σ) ($N = 7$). For the details of the method, see *Liang et al.* [2003].

4. Field Occurrences of the Lichi Mélange

For convenience of description, we further divide the Mukeng-Chi section into three sectors (Figures 3, 8, and 9). The Mukeng-Chi section is dominated by the broken formation facies and characterized by the intercalation of intensely sheared muddy matrix and weakly sheared turbidities (Figures 5a–5d and 5f–5g). However, the block-in-matrix mélange bearing basic-ultrabasic blocks rarely appears (Figure 5e). The most peculiar lithological feature is the intensely sheared muddy matrix without distinct stratification (Figure 5c). The muddy matrix is penetrated by scaly foliation primarily dipping to the southeast [*Chang et al.*, 2000], and the curviplanar surfaces of the scaly foliation are generally polished and bear slickensides (Figure 5d). The turbidite sequences alternating with the muddy matrix predominantly consist of sandstone/shale interbeds, but

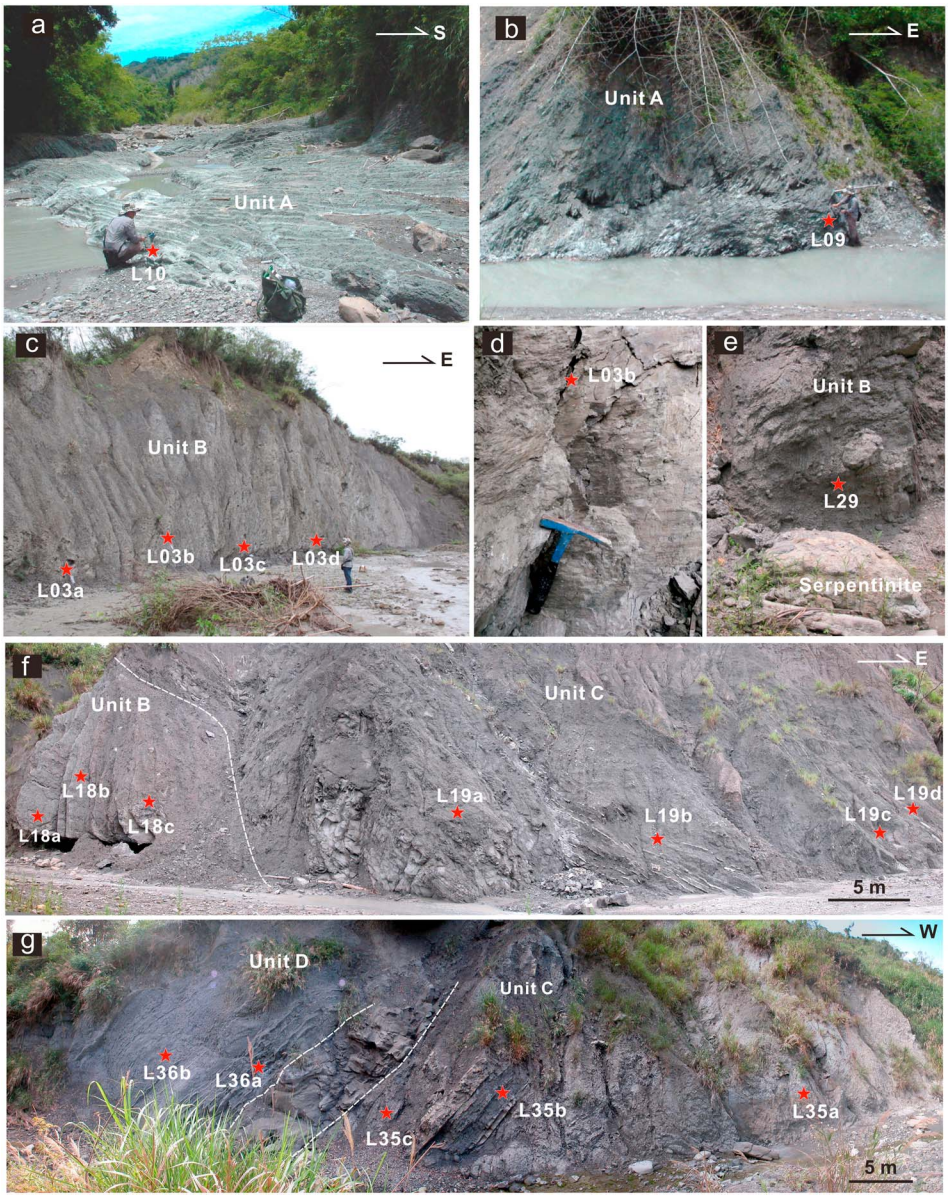

Figure 5. Field occurrences of broken formations (Figures 5a–5d, 5f, and 5g) and block-in-matrix mélanges (Figure 5e) in the Lichi Mélange along the Mukeng-Chi section. (a) Weakly disturbed greenish volcaniclastic turbidites with internal strata continuity of Unit A (<8.5–6.4 Ma) in Sector 1. (b) Highly sheared greenish volcaniclastic turbidites without discernable bedding of Unit A in Sector 1. (c) Intensively sheared muddy matrix of Unit B (6.4–5.5 Ma) in Sector 1. (d) A close-up view of Site L03b showing a polished surface with slickensides of the scaly foliation penetrating into the muddy matrix. (e) Intensively sheared muddy matrix with an exotic serpentinite block of Unit B in Sector 2. (f) In Sector 1, the highly sheared muddy matrix of Unit B in the west grades into the weakly sheared calcareous volcaniclastic turbidites of Unit C (5.5–3.4 Ma) in the east. In particular, abundant reworked early Miocene planktonic foraminifera are found at Site L18b. (g) In Sector 3, bounded by the quartzose sandstone slab (outlined by dashed line), the west shows an intensively sheared muddy matrix of Unit C with a small outcrop with remnant bedding (at Site L35b), while the east shows weakly disturbed turbidites of Unit D (3.4–3.0 Ma) rich in slate fragments similar to the Takangkou Formation.

conglomerates and pebbly mudstones are also found locally. Although the turbiditic rocks are commonly sheared, the bedding is still traceable, and the thickness is up to hundreds of meters. The contacts between the turbidites and the matrix vary in nature. Locally, faults dipping to the east are well exposed, but in general cases, there is no sharp boundary between the turbidites and the matrix, only a gradual change (e.g., Figure 5f). It is noteworthy that an arcward back thrust dipping to west was observed between Sites L04a and L05 [*Chang et al.*, 2000] (Figure 3). The Lichi Mélange is overthrust westward onto the Holocene alluvial conglomerates along the Logitudinal Valley Fault and is overthrust by the normal sequences of the Taiyuan remnant forearc basin along the Tuluanshan Fault (Figure 3).

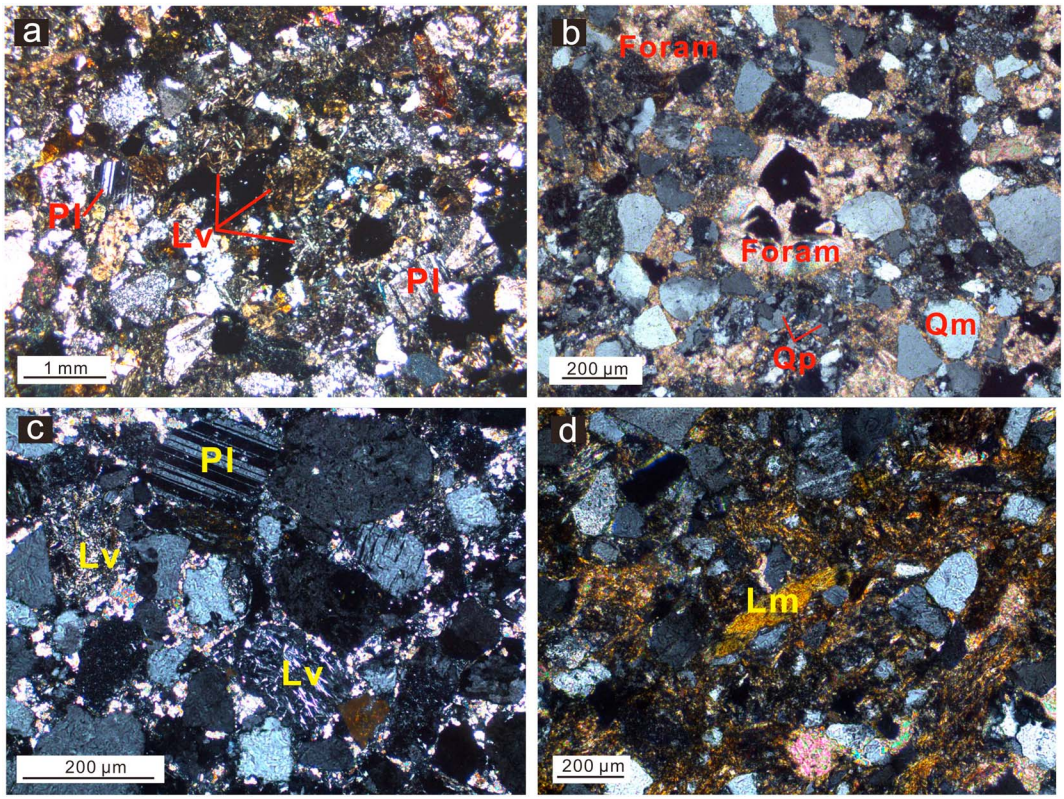

Figure 6. Photomicrographs of sandstones in the broken formation of the Lichi Mélange along the Mukeng-Chi section. (a) Sandstone of Unit A with abundant plagioclase (Pl) and volcanic lithic fragments (Lv). (b and c) Sandstones of Unit C with foraminiferal tests (Foram), monocrystalline quartz (Qm), polycrystalline quartz (Qp), volcanic lithic fragments (Lv), and plagioclase (Pl). (d) Sandstone of Unit D with slate fragments (Lm).

Notably, three huge blocks of turbidites with distinct lithologies are found along the Mukeng-Chi section. The first block is the greenish-gray volcaniclastic turbidites in the middle part of Sector 1 (Sites L07 to L12). Most of the outcrops show continuous stratification (Figure 5a), and sedimentary slump folds are locally found. The sandstone beds contain voluminous volcanic fragments and plagioclase, indicating a considerable input of arc-derived material (Figure 6a). Plagioclase crystals are mostly fresh, euhedral to subhedral, and lath like, but some are highly altered. Volcanic fragments are dominated by andesites with porphyritic texture. Hornblende and monocrystalline quartz are also found in fine-grained sandstone. In some outcrops, the rocks are boudinaged and even sheared into the muddy matrix (Figure 5b). A similar but smaller block is found in the easternmost tip of Sector 3 (Site L42) (Figure 3). The second block is the calcareous volcaniclastic turbidites in the eastern Sector 1 (Sites L17 and L19). The turbidite sequences are moderately sheared and transition westward into a strongly sheared muddy matrix (Figure 5f). Foraminiferal tests, quartz, plagioclase, and volcanic clastics are observed in the sandstone beds (Figures 6b and 6c). Volcanic clastics still occur frequently, but their relative abundance is greatly reduced. The third block is the turbidites in the middle of Sector 3 (Sites L36 to L41) (Figure 5g), which are characterized by the presence of slate chips (Figure 6d) derived from the slate belt of the Central Range. The field occurrence and lithology resemble the Takangkou Formation in the remnant forearc basin.

The Lichi Mélange in the southern end and the middle part of the Coastal Range comprises mostly a typical block-in-matrix mélange bearing numerous blocks of whitish quartzose sandstone, andesitic rock, and basic-ultrabasic rocks. In the southern end of the Coastal Range, the Lichi Mélange is overthrust westward onto the late Pleistocene Pinanshan Conglomerate and the Holocene alluvial conglomerates along the Pinanshan Fault and the Lichi Fault which are branches of the Lougitudinal Valley Fault (Figure 4a). The Lichi Mélange along the downstream section of the Chunchieh-Chi appears as a broken formation of weakly sheared mudstone. Along the Tulanpi Coast, blocks of the muddy matrix of the Lichi Mélange, which might have been transported by rivers, are embedded in the modern beach sands (Figure 4a).

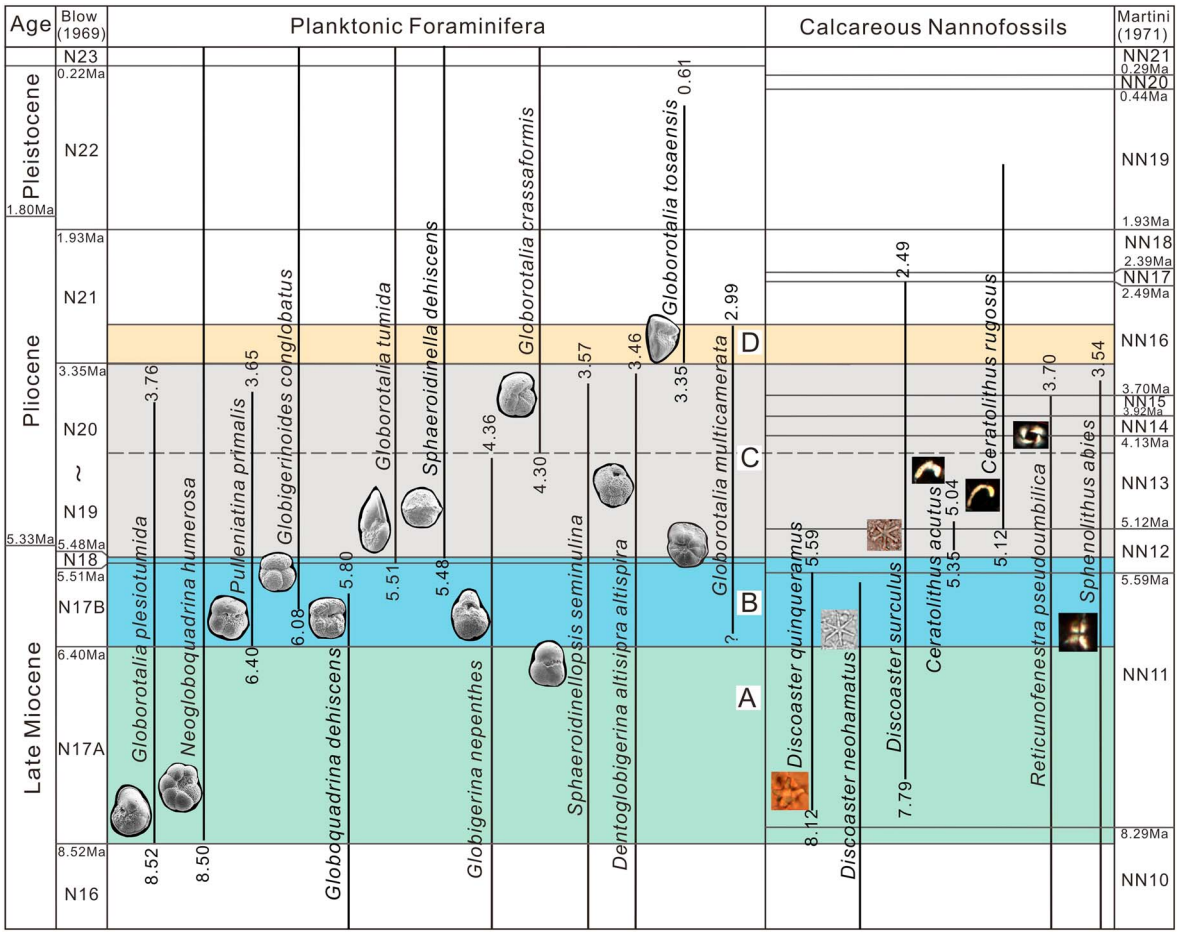

Figure 7. Datum planes of age-diagnostic microfossils in the Lichi Mélange. Datum planes of planktonic foraminifera and calcareous nannofossils are given according to *Wade et al.* [2011] and *Anthonissen and Ogg* [2012], respectively. Forearc sequences in the Lichi Mélange are chronologically divided into four units (A–D, shown in different colors) as constrained by the age-diagnostic microfossils. Unit C can be further divided into two subunits by the dashed line.

5. Biostratigraphic Result of the Lichi Mélange

5.1. Biostratigraphic Zonation

The muddy matrix of the Lichi Mélange exposed along the Ruchiang-Chi and the Peinan River in the southernmost end of the Coastal Range (Figure 4a) contains rare microfossils, making it difficult to determine its age. The Lichi Mélange in these areas presents as a typical block-in-matrix mélange and corresponds to the "Rare Fossil Zone" defined by *Chang* [1967].

In other areas of this study, represented by the Mukeng-Chi section, the muddy matrix and turbidites of the Lichi Mélange bear abundant planktonic foraminifera. These fossils are generally well preserved and dominated by warm-water fauna (Figure 10). However, calcareous nannofossils are generally present in low abundance and their preservation varies from poor to moderate (Figure 11). Here we are strongly biased toward the age-diagnostic fossils. The identified planktonic foraminifera (70 species and subspecies belonging to 13 genera) and calcareous nannofossils (40 species and subspecies belonging to 10 genera) are listed in detail in Tables S1 and S2 in the supporting information, and a brief description is also provided as Text S1. The age-diagnostic fossils are listed on the lithological columns (Figures 8 and 9) and on the geological map of the Mukeng-Chi section (Figure 12). The results show that the muddy matrix and turbidites in the Lichi Mélange (mostly broken formation) range in age from the late Miocene to the early Pliocene (Zones N17A–N21; <8.5–3.0 Ma). Based on the microfossil assemblages and field occurrences, we have delineated four biostratigraphic units in the Lichi Mélange: Unit A (<8.5–6.4 Ma), Unit B (6.4–5.5 Ma), Unit C (5.5–3.4 Ma), and Unit D (3.4–3.0 Ma) (Figure 7). On the lithological columns and the geological map of the Mukeng-Chi section, these four biostratigraphic units are presented in different colors (Figures 8, 9, and 12).

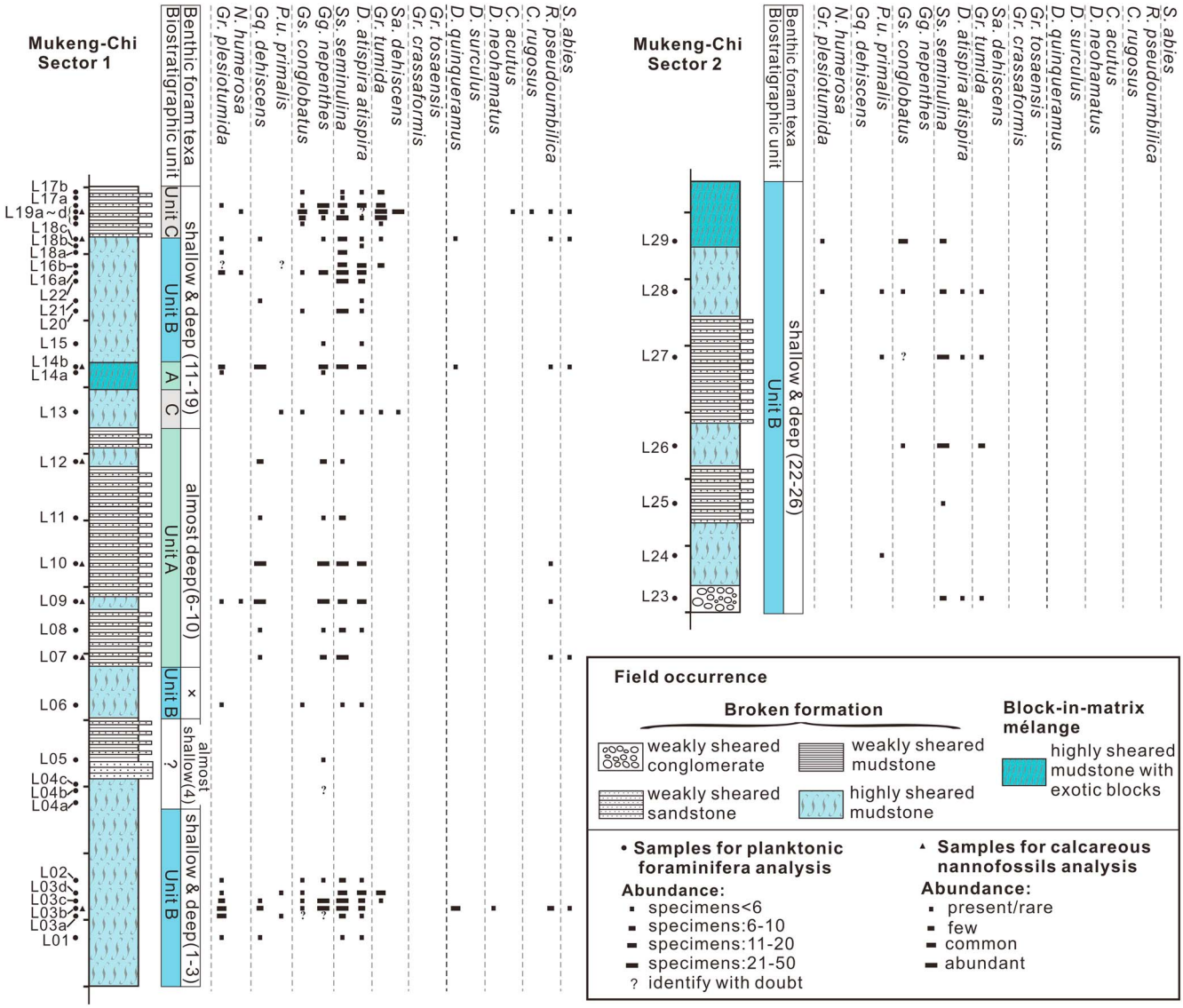

Figure 8. General lithological columns and distribution of microfossils in the Lichi Mélange exposed along Sector 1 and Sector 2 of the Mukeng-Chi section. The samples employed for planktonic foraminiferal and calcareous nannofossils analyses are marked as circles and triangles, respectively. The biostratigraphic units defined in Figure 7 are listed on the right sides of the lithological columns. The paleobathymetry of benthic foraminifera (deep sea and/or shallow marine) and the sample numbers documented by *Huang et al*. [2008] are also shown.

Unit A is composed primarily of the volcaniclastic turbidites in the center of Sector 1 and in the eastern part of Sector 3 (Figures 5a, 5b, and 12). The most striking feature of this unit is the occurrence of numerous *Globoquadrina dehiscens* (Chapman, Parr & Collins) (LAD: 5.80 Ma) which have not been reported in previous studies. There are also abundant *Globigerina nepenthes* Todd, *Globigerinoides obliquus* Bolli, *Globigerinoides extremus* Bolli & Bermúdez, *Orbulina suturalis* Brönnimann, *Orbulina bilobata* (d'Orbigny), *Globorotalia limbata* (Fornasini), *Dentoglobigerina altispira altispira* (Cushman & Jarvis), *Neogloboquadrina acostaensis* (Blow), *Sphaeroidinellopsis seminulina* (Schwager) and *Sphaeroidinellopsis subdehiscens* Blow and a few *Globorotalia lenguaensis* Bolli (LAD: 6.00 Ma), *Globoquadrina baroemoenensis* (LeRoy), and *Sphaeroidinellopsis kochi* Caudri. These species constitute a typical late Miocene assemblage. The appearance of *Globorotalia plesiotumida* Blow & Banner (FAD: 8.52 Ma) and *Neogloboquadrina humerosa* (Takayanagi & Saito) (FAD: 8.50 Ma) and the absence of *Pulleniatina primalis* Banner & Blow (FAD: 6.40 Ma) and *Globigerinoides conglobatus* (Brady) (FAD: 6.08 Ma) indicate an age of Zone N17A (<8.5–6.4 Ma) (Figures 7–9). Calcareous nannofossils in this unit are found in low abundance and dominated by species appearing since the late Miocene: *Catinaster coalitus* Martini & Bramlette (NN8–NN9; FAD: 10.89 Ma; LAD: 9.69 Ma), *Discoaster bollii* Martini & Bramlette

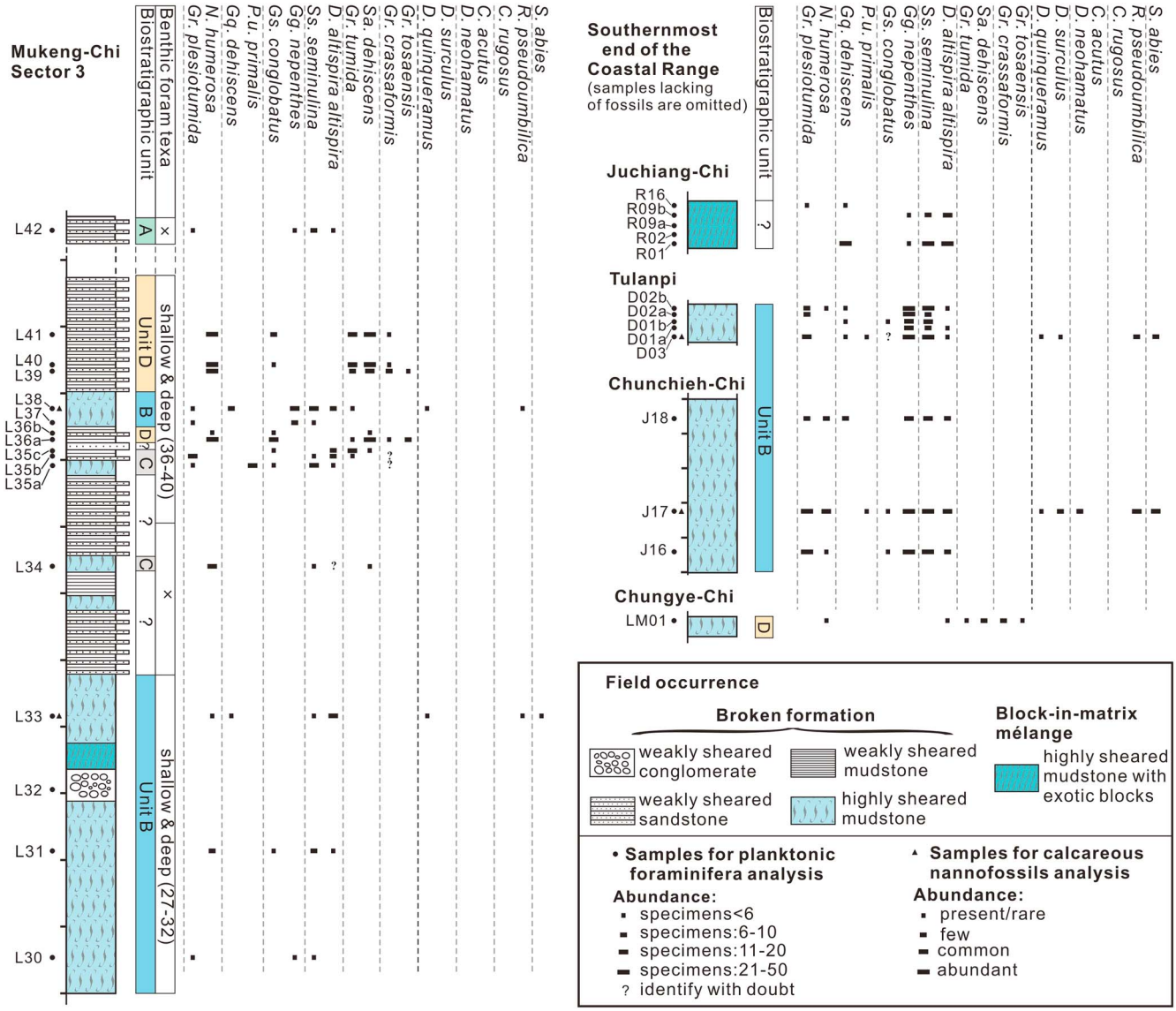

Figure 9. General lithological columns and distribution of microfossils in the Lichi Mélange exposed along Sector 3 of the Mukeng-Chi section and in the southernmost end of the Coastal Range. Those samples lacking planktonic foraminifera along the Juchiang-Chi and Peinan River sections are omitted. See the caption for Figure 8 for an explanation of symbols and references.

(NN8–NN10; LAD: 9.21 Ma), *Discoaster brouweri* Tan (NN8–NN19; FAD: 10.76 Ma), *Discoaster pentaradiatus* Tan (NN9–NN17; FAD: 9.37 Ma), *Reticulofenestra pseudoumbilica* (Gartner) (NN6–NN15; FAD: 12.83 Ma), and *Sphenolithus abies* Deflandre (NN9–NN15). There are also sporadic occurrences of *Discoaster quinqueramus* Gartner (FAD: 8.12 Ma; LAD: 5.59 M), suggesting that at least part of this unit can be assigned to Zone NN11 (Figures 7 and 8). This age is consistent with that obtained from the planktonic foraminifera. Thus, the occurrence of *C. coalitus* and *D. bollii* can be attributed to reworking.

Unit B includes most of the muddy matrix and small portions of the turbidite sequences of the Mukeng-Chi section (Figures 5c, 5e, 5f, and 12), and the muddy matrix crops out along the Chunchieh-Chi section and the Tulanpi Coast (Figure 4a). This unit yields a late Miocene foraminiferal assemblage similar to Unit A. It is noteworthy that *Pu. primalis* (FAD: 6.40 Ma) and *Gs. conglobatus* (FAD: 6.08 Ma) are observed in the samples. The abundance of *Gq. dehiscens* (LAD: 5.80 Ma) decreases significantly, but this species still occurs locally. There are also sporadic occurrences of species extending to the latest Miocene, such as *Globorotalia conoidea* Walters, *Globorotalia conomiozea* Kennett, and *Globorotalia paralenguaensis* Blow. In some samples, there are even *Globorotalia tumida* (Brady) (FAD: 5.51 Ma), whereas *Sphaeroidinella dehiscens* (Parker & Jones)

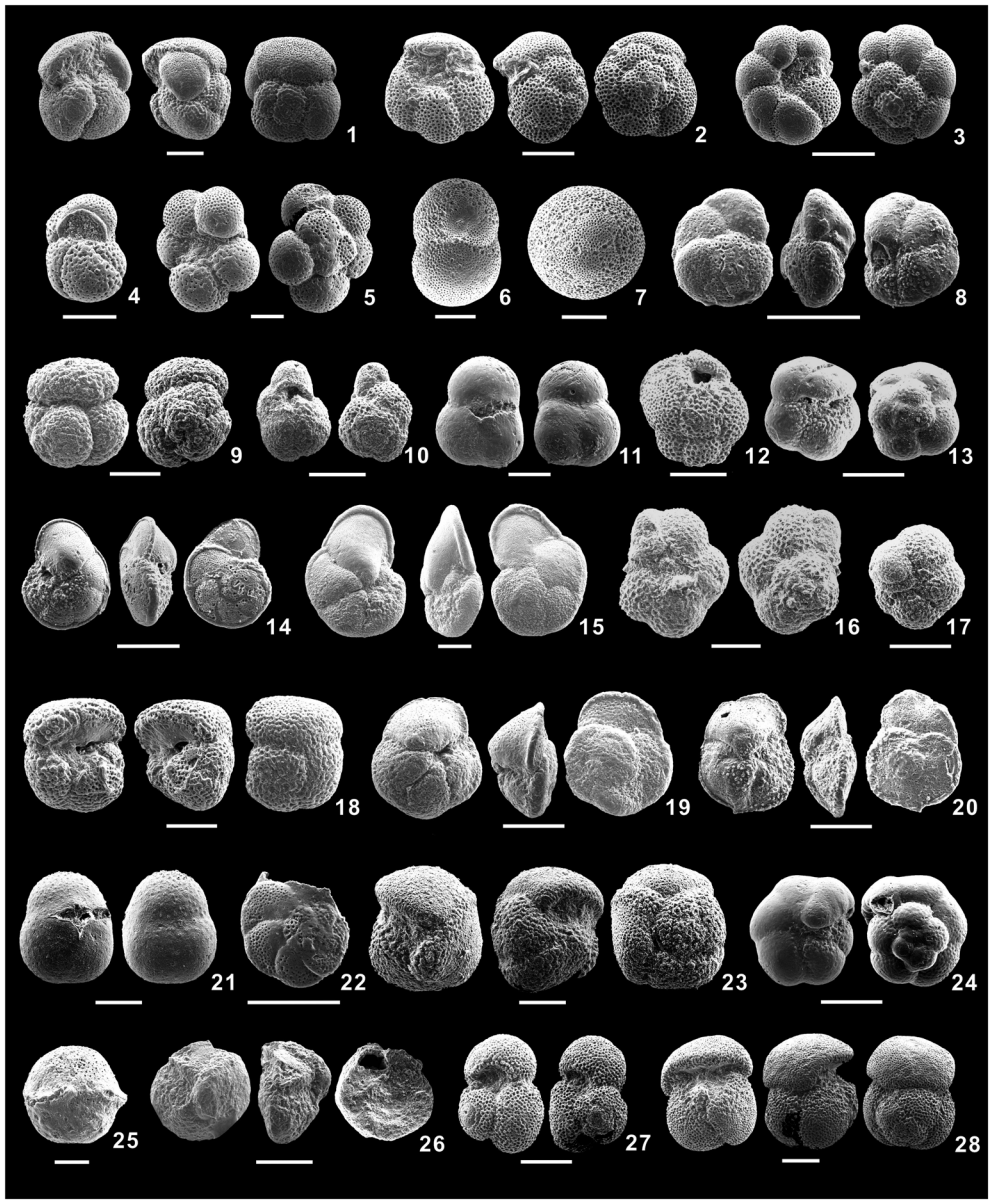

Figure 10. SEM images of planktonic foraminifera recovered from the Lichi Mélange are shown with scale bars of 200 μm. Numbers 1–8 recovered from Unit A: 1. *Globoquadrina dehiscens* (Chapman, Parr & Collins), Site L09; 2. *Globoquadrina baroemoenensis* (LeRoy), Site L09; 3. *Neogloboquadrina humerosa* (Takayanagi & Saito), Site L09; 4. *Globigerina nepenthes* Todd, Site L09; 5. *Sphaeroidinellopsis kochi* Caudri, Site L09; 6. *Orbulina bilobata* (d'Orbigny), Site L09; 7. *Orbulina suturalis* Brönnimann, Site L09; 8. *Globorotalia lenguaensis* Bolli, Site L14b. Numbers 9–24 recovered from Unit B: 9. *Globigerinoides conglobatus* (Brady), Site L03b; 10. *Globigerina nepenthes* Todd, Site L03b; 11. *Sphaeroidinellopsis seminulina* (Schwager), Site L03b; 12. *Dentoglobigerina altispira altispira* (Cushman & Jarvis), Site L03d; 13. *Pulleniatina primalis* Banner & Blow, Site L03d; 14. *Globorotalia plesiotumida* Blow & Banner, Site L03d; 15. *Globorotalia tumida* Blow & Banner, Site L03d; 16. *Sphaeroidinellopsis kochi* Caudri, Site L16a; 17. *Neogloboquadrina acostaensis* (Blow), Site L16a; 18. *Globoquadrina dehiscens* (Chapman, Parr & Collins), Site L18c; 19. *Globorotalia conomiozea* Kennett, Site L26; 20. *Globorotalia conoidea* Walters, Site L30; 21. *Sphaeroidinellopsis subdehiscens* Blow, Site J16; 22. *Globorotalia paralenguaensis* Blow & Banner, Site J16; 23. *Globoquadrina dehiscens* (Chapman, Parr & Collins); 24. *Pulleniatina primalis* Banner & Blow, Site D03. Numbers 25–26 recovered from Unit D: 25. *Sphaeroidinella dehiscens* (Parker & Jones), Site L36c; 26. *Globorotalia tosaensis* Takayanagi & Saito, Site L36a. Numbers 27–28, reworked early Miocene fossils in Unit B: 27. *Globigerinoides altiapertura* Bolli, Site L18b; 28. *Globoquadrina praedehiscens* Blow & Banner, Site L18b.

(FAD: 5.48 Ma) are never found. Therefore, Unit B can be constrained to Zones N17B–N18 (6.4–5.5 Ma) (Figures 7–9). The calcareous nannofossil assemblage of this unit resembles that found in Unit A. There are frequent appearance of *D. quinqueramus* (FAD: 8.12 Ma; LAD: 5.59 M) and sporadic occurrences of *Discoaster neohamatus* Bukry & Bramlette (NN9–NN11), *Discoaster surculus* Martini & Bramlette (FAD: 7.79 Ma), and *Discoaster intercalaris Bukry* (NN11–NN12), constraining Unit B well within Zone NN11 (8.3–5.6 Ma) (Figures 7–9).

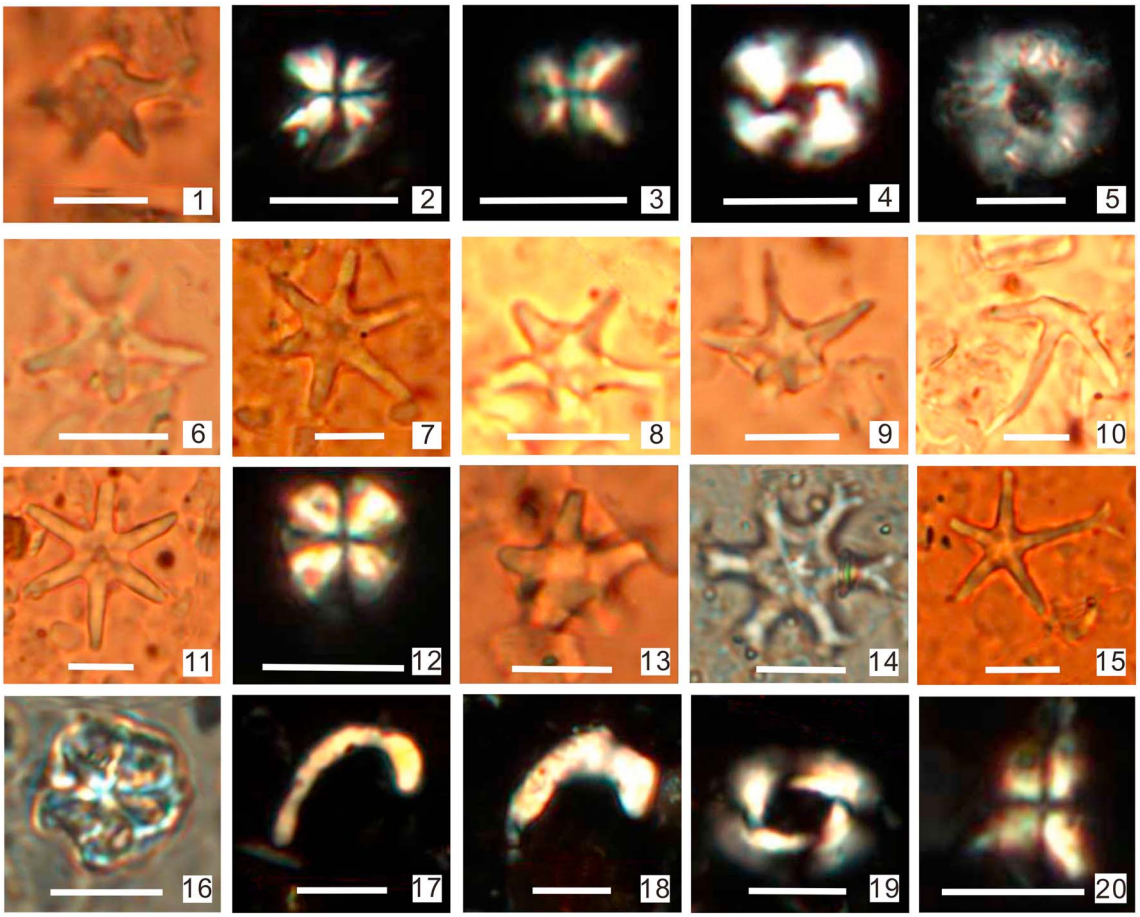

Figure 11. Polarizing photographs of calcareous nannofossils recovered from the Lichi Mélange are shown with scale bars of 5 μm. Numbers 1–7 recovered from Unit A: 1. *Discoaster bollii* Martini & Bramlette, Site L09, parallel light; 2. *Sphenolithus moriformis* Brönnimann & Stradner, Site L09, crossed nicols; 3. *Sphenolithus abies* Deflandre, Site L10, crossed nicols; 4. *Cyclicargolithus floridanus* Bukry, Site L10, crossed nicols; 5. *Calcidiscus macintyrei* Loeblich & Tappan, Site L10, crossed nicols; 6. *Discoaster quinqueramus* Gartner, Site L14b, parallel light; 7. *Discoaster brouweri* Bramlette & Riedel, Site L14b, parallel light. Numbers 8–16 recovered from Unit B: 8–9. *Discoaster quinqueramus* Gartner, Site L03b, parallel light; 10. *Discoaster neohamatus* Bukry & Bramlette, Site L03b, parallel light; 11. *Discoaster brouweri* Bramlette & Riedel, Site L03b, parallel light; 12. *Sphenolithus neoabies* Bukry & Bramlette, Site L18c, crossed nicols; 13. *Discoaster quinqueramus* Gartner, Site L38, parallel light; 14. *Discoaster intercalaris* Bukry, Site L38, parallel light; 15. *Discoaster pentaradiatus* Bramlette & Riedel, Site L38, parallel light; 16. *Catinaster coalitus* Martini & Bramlette, Site L38, parallel light. Numbers 17–20 recovered from Site L19c, Unit C: 17. *Ceratolithus rugosus* Bukry & Bramlette, crossed nicols; 18. *Ceratolithus acutus* Gartner & Bukry, crossed nicols; 19. *Reticulofenestra pseudoumbilica* Gartner, crossed nicols; 20. *Sphenolithus abies* Deflandre, crossed nicols.

The most prominent feature of Unit C is the disappearance of *Gq. dehiscens* (LAD: 5.80 Ma) and the occurrence of *Sa. dehiscens* (FAD: 5.48 Ma). There are also many *D. altispira altispira* (LAD: 3.46 Ma) and *Ss. seminulina* (LAD: 3.57 Ma). Moreover, *Globorotalia tosaensis* Takayanagi & Saito (FAD: 3.35 Ma) is generally absent. Thus, this unit can be assigned to Zones N19–N20 (5.5–3.4 Ma) (Figures 7–9). It can be further divided into two members. The lower member consists of the calcareous volcanic turbidites in eastern Sector 1 and a small part of the muddy matrix (Figures 5f and 12). The presence of *Gg. nepenthes* (LAD: 4.36 Ma) and the absence of *Globorotalia crassaformis* (Galloway & Wissler) (FAD: 4.30 Ma) suggest an age of the lower Zones N19–N20 (5.5–4.3 Ma). There are also calcareous nannofossils of *Ceratolithus acutus* Gartner & Bukry (FAD: 5.35 Ma; LAD: 5.04 Ma) and *Ceratolithus rugosus* Bukry & Bramlette (FAD: 5.12 Ma), indicating an age of approximately 5 Ma within Zones NN12–NN13 (Figures 7 and 8). The upper member is mainly distributed in the center of Sector 3 (Figures 5g and 12) and the west of the Loho remnant forearc basin [*Chen et al.*, 2015] (Figure 4b). This member can be constrained to the upper Zones N19–N20 (4.3–3.4 Ma) based on the disappearance of *Gg. nepenthes* and the appearance of *Gr. crassaformis*. Consistently, the occurrence of *Pseudoemiliania lacunosa* (Kamptner) (FAD: ~4.0 Ma) [*Gartner*, 1990], *R. pseudoumbilica* (LAD: 3.70), and *S. abies* (LAD: 3.54 Ma) indicates an age of Zones NN14–NN15 (~4.0–3.7 Ma) (Figures 7 and 9).

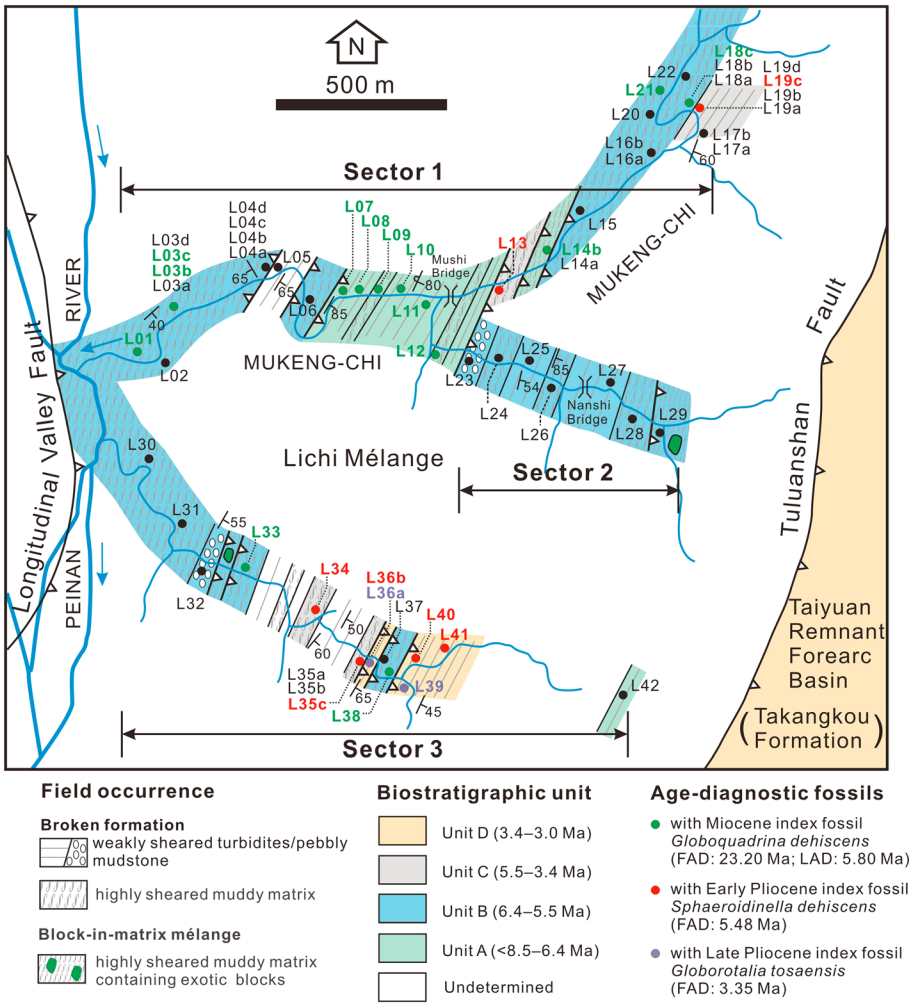

Figure 12. Biostratigraphic results plotted on the geological map of the Lichi Mélange along the Mukeng-Chi section. The thrust faults inside the mélange are based on our field observations including data of *Chang et al.* [2000] and our biostratigraphic results.

Unit D comprises the turbidites rich in slate chips in the middle of Sector 3 (Figures 5g and 12) and at Site LM 01 (Figure 4a). This unit contains planktonic foraminifera referable to lower Zone N21 (3.4–3.0 Ma) (Figures 7 and 9), characterized by the concurrent occurrence of *Gr. tosaensis* (FAD: 3.35 Ma) and *Globorotalia multicamerata* Cushman & Jarvis (LAD: 2.99 Ma). In addition, *D. altispira altispira* (LAD: 3.46 Ma) and *Ss. seminulina* (LAD: 3.57 Ma) are no longer observed.

5.2. Reworked Fossils

Most of the planktonic foraminifera recovered from the Lichi Mélange are indigenous fossils. They are well preserved, white to cream in color, and slightly petrified. The exceptions to this pattern are the reworked fossils found in Sites L18b, L20, and L21 in Unit B (Figure 10), such as *Globigerinoides altipertura* Bolli (N5–N7; FAD: 20.50 Ma), *Catapsydrax dissimilis* (Cushman & Bermúdez) (P13–N6; LAD: 17.62 Ma), *Globoquadrina praedehiscens* Blow & Banner (P22–N6), *Globorotalia mayeri* Cushman & Ellisor (N4A–N14), and *Globigerinella praesiphonifera* (Blow) (N4B–N13). This association indicates an early Miocene age (Zones N5–N6, 20.5–17.6 Ma). Unlike the indigenous fossils, these reworked fossils are poorly preserved, brown to dark brown in color, and highly petrified. However, calcareous nannofossils of diverse ages, e.g., *Dictyococcites hesslandii* (Haq) (NP18–NP24; late Eocene to early Oligocene), *Sphenolithus moriformis* Brönnimann & Stradner (NP11–NN8; Eocene to late Miocene), *Sphenolithus heteromorphus* Deflandre (NN4–NN5; middle Miocene), *Cyclicargolithus abisectus* (Müller) (NP24–NN1; Oligocene), and *Cyclicargolithus floridanus* (Roth & Hay) (NP20–NN6; late Eocene to middle Miocene), frequently appear in the samples of each unit.

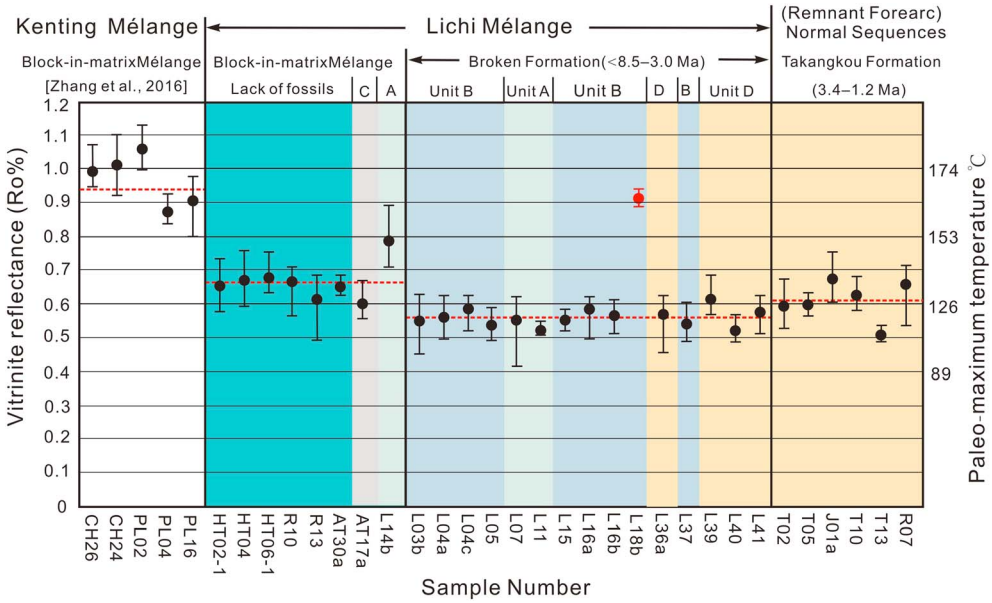

Figure 13. Paleothermal structure of the Lichi Mélange and the normal sequence in the remnant forearc basin determined from vitrinite reflectance (Ro) compared with the Kenting Mélange in the Hengchun Peninsula [*Zhang et al.*, 2016]. The bars show the range of data for each sample. Temperature is estimated according to the approach of *Sweeney and Burnham* [1990]. Sample L18 marked in red with an age of early Miocene is interpreted as having a reworked origin. The red dashed lines represent the mean values.

6. Vitrinite Reflectance and Nd Isotope Results

6.1. Vitrinite Reflectance

The results of vitrinite reflectance (Ro) of the sediment samples are listed in Table S3 in the supporting information and Figure 13 according to the field occurrences and sedimentary ages (see Figures 3 and 4 for the sampling sites). In general, the samples possess Ro values between 0.4% and 0.8%, except for an abnormally high value (0.91%) for L18b of the broken formation. Since this sample yields abundant early Miocene reworked fossils, the abnormally high value might be derived from reworked vitrinites of the older strata. Therefore, this value is removed from further discussion. Generally, there are no obvious variations in Ro values between the stratigraphic units with different degrees of deformation. Ro values of the normal sequences in the remnant forearc basin range from 0.5% to 0.7% (average 0.61), whereas those of the broken formation and block-in-matrix mélange in the Lichi Mélange range from 0.5% to 0.6% (average 0.56%) and from 0.6% to 0.8% (average 0.66%), respectively.

6.2. Nd Isotopes

The results of Nd isotope analysis on the sediment samples are listed in Table S4 in the supporting information (see Figures 3 and 4 for the sampling sites). The $^{143}Nd/^{144}Nd$ ratios range from 0.511997 to 0.512222, corresponding to a εNd range from -12.5 to -8.1 (Figure 14). The εNd values can be divided into two groups well correlated with the depositional age. The sediments of Unit A in the Lichi Mélange ($<$8.5–6.4 Ma; volcaniclastic turbidites) possess higher εNd values, ranging from -11.0 to -8.1 (with an average of -9.2), whereas the sediments younger than 6.4 Ma (including Units B–D in the Lichi Mélange and the remnant forearc sequences) have obviously lower εNd values, concentrated in the range from -12.5 to -11.9 (with an average of -12.3).

7. Discussion

7.1. Significance of the Biostratigraphic Reconstruction

7.1.1. Discrimination of the Reworked Fossils in the Lichi Mélange

The late Miocene fossils in the Lichi Mélange have often been attributed to reworking in previous studies [*Huang*, 1969; *Chi et al.*, 1981; *Chi*, 1982; *Barrier and Muller*, 1984]. Here we also found numerous late Miocene fossils in Units A and B of the Lichi Mélange. Nevertheless, these late Miocene fossils are well

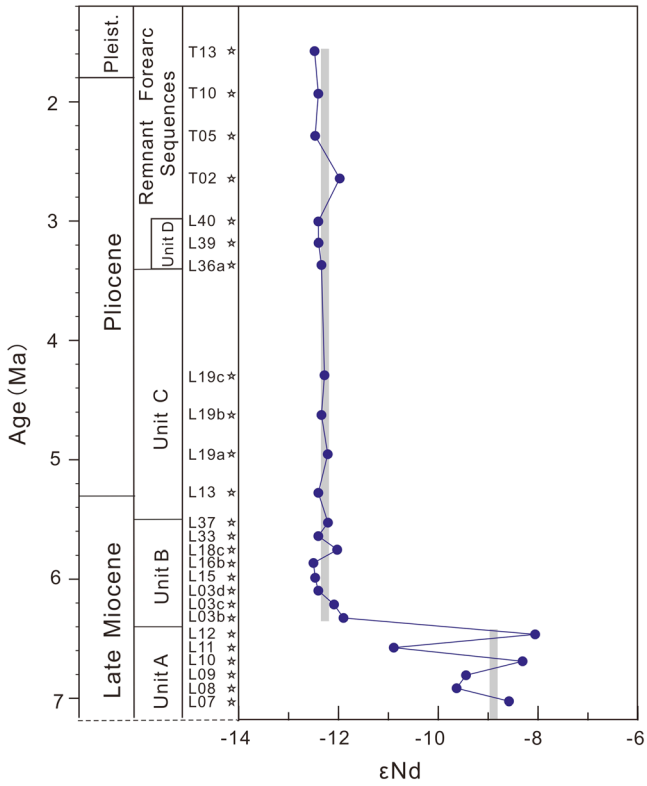

Figure 14. The profile variations of Nd isotopic composition of mudstones collected from the forearc basin (the Lichi Mélange and the remnant forearc basin). The absolute ages of the samples on the profile are estimates due to the limitation of the biochronology and the discontinuity of the strata.

preserved and do not occur concurrently with younger fossils in the same sample, and the depositional ages of Units A and B are well constrained by the integration of planktonic foraminifera and calcareous nannofossils. Moreover, evidence of mass slumping is rarely observed in these two units. Therefore, the late Miocene fossils should be treated as indigenous fossils instead of reworked fossils. In contrast, early Miocene reworked planktonic foraminifera are found in Unit B. These fossils appear together with the younger faunas in the same sample/outcrop and might be derived from the erosion of the sedimentary cover of the Central Range accretionary prism.

Two reasons might account for the misinterpretation of the late Miocene fossils by previous researchers. First, they dated the Lichi Mélange simply using the samples bearing younger fossils under the influence of the olistostromal origin hypothesis and thus considered the older fossils as reworked fossils, overlooking the field occurrences and fossil assemblages. Second, calcareous nannofossils in the sediments are prone to be polluted through various geological processes and during sample treatment due to their tiny size; it is not unusual for calcareous nannofossils to become contaminated by fossils displaced from the older strata. Furthermore, the Lichi Mélange with its widespread faults may have acquired younger nannofossils when they were exposed on the seafloor or on land [*Jones*, 1958]. The older indigenous fossils would thus be misinterpreted as reworked fossils. For example, we found rare *P. lacunosa* (FAD: ~4.0 Ma) [*Gartner*, 1990] and a single specimen of medium *Gephyrocapsa* spp. (FAD: 1.67 Ma) indicative of Pleistocene age, at Site J17, downstream from the Chunchieh-Chi (Figure 4a), but other than these two species, the microfossil assemblages suggest an age of late Miocene (Unit B). Therefore, we infer that the two species were eroded from the Pleistocene Takangkou Formation exposed upstream and were then mixed into the Lichi Mélange.

7.1.2. Origin of the Lichi Mélange

The Lichi Mélange has been interpreted as an olistostrome deposited in the western part of the forearc basin by eastward mass wasting from the exposed accretionary prism during arc-continent collision [*Wang*, 1976; *Page and Suppe*, 1981; *Barrier and Muller*, 1984]. In this interpretation, this mélange might register one or several rapid tectonic events related to the collision. In contrast, under the tectonic origin model of the Lichi Mélange which is primarily generated from the shearing of the normal forearc basin sequences [*Chang et al.*, 2000, 2001; *Huang et al.*, 2000, 2008], we can obtain a long-term sedimentary record of the forearc basin. Therefore, the different interpretations of the origin of the Lichi Mélange might result in different understandings of the history of the Taiwan arc-continent collision.

In the olistostrome model, the Lichi Mélange represents a chaotic facies coeval with the Takangkou Formation, and the contact between them is quasi-conformable with some evidence for interfingering [*Page and Suppe*, 1981]. However, our biostratigraphic data indicate that the forearc sequences in the

Lichi Mélange were formed during <8.5–3.0 Ma, whereas the Loho, Taiyuan, and Taitung remnant forearc basins in the east developed during 3.4–1.2 Ma [*Horng and Shea*, 1996; *Chen et al.*, 2015]. Obviously, most of the forearc sequences preserved in the Lichi Mélange are older than the remnant forearc sequences (Takangkou Formation), and thus, the Lichi Mélange cannot be an olistostromal facies coeval with the remnant forearc sequences. More than 100 m thick pebbly mudstone layers generated from gravitational slumping or debris flow commonly occur within the Takangkou Formation. *Page and Suppe* [1981] have argued that the Lichi Mélange and these pebbly mudstone layers (or olistostromes) contain similar fossil assemblages and therefore have the same origin. However, the fossil assemblages in the pebbly mudstone are distinct from those in the Lichi Mélange, which thus contradicts the olistostromal origin of the Lichi Mélange. The late Pliocene (3.4–3.0 Ma) indigenous fossils in the pebbly mudstone in the Loho remnant forearc basin appear together with late Miocene to early Pliocene reworked fossils in the same sample [*Chen et al.*, 2015]. The pebbly mudstone in the Taitung remnant forearc basin includes Pleistocene indigenous fossils together with late Miocene to early Pliocene reworked fossils [*Chen et al.*, 2015].

Based on our biostratigraphic data, we infer that the four units in the Lichi Mélange constitute a set of continuous sequences (<8.5–3.0 Ma) (Figure 7). Additional evidence is that some evolutionary trends of the late Miocene to early Pliocene planktonic foraminifera can still be observed. The development of *Gr. tumida* from *Gr. plesiotumida* at ~5.51 Ma is observed at Site L03 of Unit B, although the mudstone has been highly sheared (Figures 5c and 8). The first appearance of *Sa. dehiscens* at ~5.48 Ma can be observed between Sites L18 and L19, where the highly sheared muddy matrix of Unit B grades into the weakly sheared turbidites of Unit C (Figures 5f and 8). These observations suggest the continuity of the original strata forming the Lichi Mélange. Therefore, our dating results support the interpretation that the Lichi Mélange arose from the lower sedimentary sequences of the forearc basin [*Chang et al.*, 2000, 2001; *Huang et al.*, 2000, 2008]. Nevertheless, we do not deny the local occurrence of olistostromes in the Lichi Mélange, as evidenced by slumping folds locally observed in Unit A, the reworked early Miocene fossils found at Sites L18b, L20 and L21 of Unit B, and the pebbly mudstones found at Sites L23 and L32 of Unit B. *Chi et al.* [2014] also suggested that slumping triggered by gravitational failure might widely occur in the Lichi Mélange when the lower forearc sequences were uplifted and formed the bathymetric high by eastward back thrusting (see section 7.2.1).

Previous studies showed that the East Taiwan Ophiolite in the Lichi Mélange was originated from the South China Sea [*Jahn*, 1986; *Chung and Sun*, 1992]. However, a recent study based on zircon U-Pb dating and Hf isotope analysis on gabbros, diorites, and plagiogranites suggested that the East Taiwan Ophiolite originated from the highly depleted forearc magma due to forearc spreading during the initiation of the South China Sea subduction [*Shao*, 2015]. The U-Pb dating results showed a range of 17.5–14.1 Ma [*Shao*, 2015], well correlating with the earliest vocalism of the North Luzon Arc (~16 Ma) [*Yang et al.*, 1988, 1995; *Lo et al.*, 1994]. Thus, the blocks of basic and ultrabasic rocks might represent the arc-forearc basement formed in the upper plate and then incorporated into the Lichi Mélange during the arc-continent collision. Between this ophiolitic basement and the oldest forearc sediments dated in the Lichi Mélange (Unit A) could be the andesitic agglomerates of the volcanic arc, which were also emplaced into the Lichi Mélange. The emplacement of these ophiolitic and andesitic blocks into the Lichi Mélange could occur as young as ~1 Ma [*Huang et al.*, 2008].

7.2. Effects of Back Thrusting on Forearc Sedimentation

7.2.1. Correlation Between Offshore and Onshore Geology

A general geological feature of the forearc stratigraphy in the Coastal Range is that the older Lichi Mélange occurs to the west of the younger remnant forearc sequences. However, it is difficult to understand why the younger forearc sequences could locally be thrust westward over the older Lichi Mélange along the Tuluanshan Fault. What occurred on the lower forearc basin sequences in the Lichi Mélange before the westward thrusting event? Due to a southward propagation of the oblique arc-continent collision [*Suppe*, 1981], we can use the present geological situation of a southern segment to reconstruct the past framework of a northern segment. Thus, the North Luzon Trough off SE Taiwan in the incipient arc-continent collision zone provides us with a window into the tectonic-sedimentary evolution of the forearc basin in the Coastal Range. Here we refer to two recently published multichannel seismic profiles across the North Luzon Trough: GMGS 973 [*Huang et al.*, 2008] and MW9006–16 [*Hirtzel et al.*, 2009; *Chi et al.*, 2014] (Figures 1 and 15).

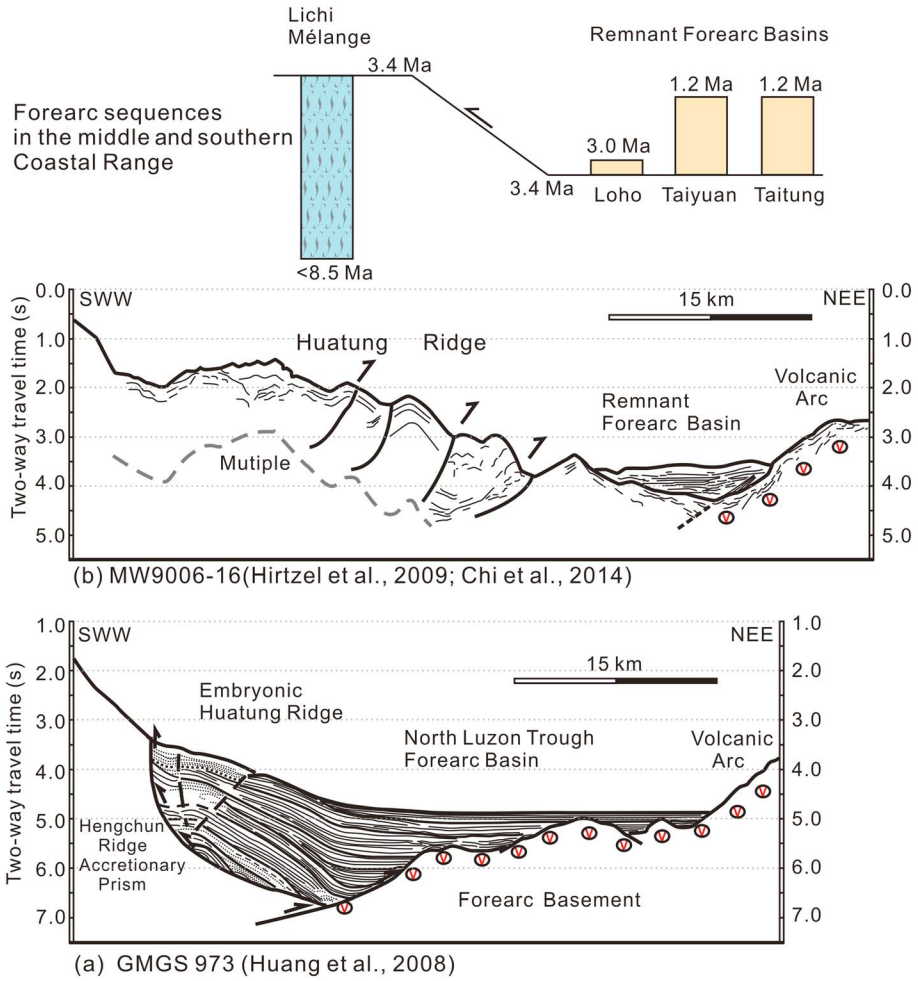

Figure 15. Two seismic profiles across the North Luzon Trough forearc basin off southeastern Taiwan; for the locations, see Figure 1. (a) Profile GMGS 973 [*Huang et al.*, 2008] in the subduction-collision transition zone showing the development of the embryonic Huatung Ridge. (b) Profile MW9006-16 [*Hirtzel et al.*, 2009; *Chi et al.*, 2014] in the incipient arc-continent collision zone compared with the distribution characteristics of the sedimentary sequences in the Coastal Range.

Profile GMGS 973 across the subduction-collision transition zone shows that the western part of the forearc basin is deformed by bivergent thrusting: westward thrusting along a high-angle east dipping boundary fault between the forearc basin and the accretionary prism and eastward back thrusting along a low-angle west dipping forearc basement. This bivergent thrust mechanism produced a pop-up structure to form the embryonic Huatung Ridge [*Huang et al.*, 2008] (Figure 15a). Younger synorogenic sediments are accumulated in the undeformed forearc basin to the east of this embryonic Huatung Ridge (Figure 15a). To the north, Profile MW9006-16 in the initial arc-continent collision zone shows that back thrusting cuts through the seafloor and migrates eastward progressively as the collision proceeds (Figure 15b). The middle and eastern parts of the forearc basin have been deformed and uplifted as the Huatung Ridge on the order of 1000 m [*Reed et al.*, 1992; *Lundberg et al.*, 1997; *Huang et al.*, 2008]. To the east of this bathymetric high, sedimentation continues in a remnant forearc basin. Sediments in this basin are relatively flat lying and only slightly deformed (Figure 15b). Therefore, it can be inferred that the Huatung Ridge in the west is older than the remnant forearc sequences.

In the middle and southern Coastal Range, the spatial-temporal variations in the forearc stratigraphy resemble those observed from the Huatung Ridge-remnant forearc basin in the deformed North Luzon Trough (Figure 15b), indicating that back thrusting might have occurred synchronously with deposition. It is likely that the back thrusting played an important role in an early stage and contributed to the uplift of the lower forearc basin sequences (the Lichi Mélange). In the later stage, strong shortening and westward thrusting led to a rearrangement of the regional structural framework. This multistep tectonic evolution thus explains why

the younger remnant forearc sequences could be locally thrust over the older Lichi Mélange along the Tuluanshan Fault. Although other mechanisms could also be responsible for the uplift of the Lichi Mélange in the early stage, the fact that the offshore Huatung Ridge is morphologically continuous northward to the Lichi Mélange [*Huang et al*., 1992] strongly supports the occurrence of the back thrusting. Westward vergent fold and thrust structures are now dominant in the Lichi Mélange, and most of the back thrusts might have been cut and replaced by the westward thrusts. Nevertheless, some back thrusts are still preserved in the field outcrops of the Lichi Mélange, such as the back thrust between Sites L04 and L05 in the Mukeng-Chi section (Figure 3) and the Yungfong Fault in the Biehhsi section reported by *Chang et al*. [2000, 2001]. A comprehensive tectonic analysis of the shear surfaces within the Lichi Mélange undertaken by *Chang et al*. [2000] indicated a strong N100°–120°E trending compression consistent with the direction of plate convergence. However, a few sites revealed extension, which can be explained by the vertical extrusion of the layers at depth [*Chang et al*., 2000]. They first underwent widespread tectonic compression and locally experienced extension when they came close to the surface because of block exhumation and wrapping. We infer that this kind of stress evolution was likely a result of the back thrusting of the lower forearc basin sequences.

As the oldest sediments in the slightly deformed remnant forearc basins in the middle and southern Coastal Range are younger than 3.4 Ma, the initiation of back thrusting should be no later than ~3.4 Ma. Units A–C (<8.5–3.4 Ma) in the Lichi Mélange are thus equivalent to the Huatung Ridge arising from the deformation of the lower forearc sequences by back thrusting (Figure 15b). These units might have initially accumulated in the depression in the western part of the forearc basin. After ~3.4 Ma, the cessation or waning of the back thrusting allowed the sedimentation of normal sequences in the remnant forearc basins in the east. Given that the youngest unit (Unit D, 3.4–3.0 Ma) in the Lichi Mélange is similar both lithologically and temporally to the lower part of the remnant forearc basins (3.4–1.2 Ma), it might represent the remnant forearc sequences emplaced into the Lichi Mélange during the advanced collision stage in the last ~1 Ma. During this stage, the Huatung Ridge was further thrust westward and sheared into the Lichi Mélange, and the remnant forearc basins and the volcanic arc in turn thrust over the Lichi Mélange [*Chang et al*., 2000, 2001; *Huang et al*., 2008]. Meanwhile, a slice of arc-forearc basement subducted eastward under the oceanic lithosphere constituting the upper plate, which could be responsible for the drastic reduction of the forearc domain in the advanced collision zone and has been demonstrated by physical and numerical modeling at lithospheric scale [e.g., *Tang and Chemenda*, 2000; *Chemenda et al*., 2001; *Malavieille and Trullenque*, 2009] and geological and geophysical observations [e.g., *Malavieille et al*., 2002; *McIntosh et al*., 2005].

7.2.2. Tectonic Implications of Vitrinite Reflectance

Vitrinite reflectance is an effective indicator of maximum temperatures during thermal diagenesis due to the irreversibility of maturation of organic material [e.g., *Tissot and Welte*, 1984]. For complicated fault systems such as fold-thrust belts and mélanges, vitrinite reflectance can be used to estimate the tectonic burial depths and cumulative displacements of the hanging wall and footwall and applied as a geothermometer for frictional heating associated with faulting [*Orange and Underwood*, 1995; *Harris et al*., 2000; *Sakaguchi et al*., 2007]. Therefore, we utilized vitrinite reflectance analysis on the normal sequences in the remnant forearc basin and the broken formation and block-in-matrix mélange in the Lichi Mélange to obtain the burial history and the tectonic evolution of the Coastal Range forearc basin.

The results of vitrinite reflectance show no obvious variations between the different facies of stratal fragmentation (Table S3 and Figure 13), indicating that the analyzed samples are not influenced by fault-related frictional heating. Instead, most of our samples may have been influenced mainly by burial depth. Due to a higher degree of deformation and mixing, the higher Ro values of the block-in-matrix mélange, especially that of sample L14b, may have resulted from the diffusion of frictional heat.

Two most popular methods for calculation of maximum temperature from vitrinite reflectance are from *Barker* [1988] and *Sweeney and Burnham* [1990] [e.g., *Sakaguchi*, 1999; *Yamamoto et al*., 2005; *Mukoyoshi et al*., 2006]. The equation of *Barker* [1988] is independent of heating time. The heating time is defined as the period between the maximum temperature and a temperature of 15°C lower than this maximum temperature [*Sekiguchi and Hirai*, 1980]. However, the stabilization of the vitrinite reflectance evolution in burial heating systems might require up to 10 Ma [*Barker*, 1989]. Taking this into account, the equation of *Barker* [1988] is not suitable for our samples with such young sedimentary ages of <8.5–1.2 Ma. The equation of *Sweeney and Burnham* [1990] is accurate for the heating time, and this time is typically 1 Myr to 10 Myr on

active margins [*Laughland and Underwood*, 1993; *Ohmori et al.*, 1997]. Considering the young ages of the samples, we estimate the maximum temperatures using the equation of *Sweeney and Burnham* [1990] with heating time of 1 Myr: T (°C) = 174 + (93[ln percentage Ro]) (Table S3 and Figure 13). The error of the equation is ±30°C in temperature. Then, the burial depth is roughly estimated assuming a 15°C surface temperature and ~40 °C/km thermal gradient (Table S3). For the latter, we adopt the present thermal gradient of the North Luzon Trough [*Chi and Reed*, 2008].

Accordingly, the burial depths are estimated to be between 2.4 and 3.1 km for the normal sequences of the remnant forearc basin (average 2.8 km), between 2.5 and 2.8 km for the broken formation (average 2.6 km), and between 2.8 and 3.4 km for the block-in-matrix mélange (average 3.0 km). The broken formation contains most of Units A–D (<8.5–3.0 Ma). However, its burial depth is close to and even shallower than that of the younger remnant forearc sequences. This observation indicates that the lower forearc sequences in the Lichi Mélange did not experience deep burial relative to the remnant forearc sequences and that they were uplifted and exhumed shortly after their deposition. This phenomenon was very likely a result of back thrusting analogous to the situation in the North Luzon Trough.

In addition, the Ro values of the Lichi Mélange are generally lower than those of the Kenting Mélange on the Hengchun Peninsula (0.8–1.0%, 0.94% on average) [*Zhang et al.*, 2016] (Figure 13). The Kenting Mélange represents a subduction channel assemblage in the bottom of the accretionary prism [*Zhang et al.*, 2016]. This comparison implies that the Lichi Mélange should have formed in a much shallower structural position than the Kenting Mélange.

7.3. Provenance Evolution of the Forearc Basin and Emergence of the Accretionary Prism

7.3.1. Nd Isotope Response to Provenance Change

Sm-Nd isotopes are effective tools to investigate the source of sedimentary rocks because Nd isotopic compositions of sediments are largely unaltered by processes of weathering, erosion and deposition [*McCulloch and Wasserburg*, 1978; *Goldstein et al.*, 1984]. Thus, Nd isotope analysis is useful to study the provenance evolution of the Coastal Range forearc basin and to test the two possible provenances, the Taiwan accretionary prism and the North Luzon Arc, which possess distinct Nd isotopic compositions (Figure 16). The εNd values of sediments and metasediments of the Taiwan accretionary prism range from −16.2 to −6.8 with a main peak at approximately −12 (compiled from the Central Range-Hsüehshan Range and the Hengchun Peninsula) [*Chen et al.*, 1990a; *Lan et al.*, 2002; *Zhang et al.*, 2014]. There are two minor peaks between −10 and −6, representing the Jurassic metasedimentary rocks of the Tailuko belt in the eastern flank of the Central Range [*Lan et al.*, 2002]. In contrast, the volcanic rocks of the North Luzon Arc show more variable εNd values, ranging from −6.7 to 10.1 (compiled from the Tuluanshan Formation in the Coastal Range and the Lutao-Lanyu Islands) [*Chen et al.*, 1990b; *Defant et al.*, 1990; *Lai et al.*, 2008, 2017; *Lai and Song*, 2013].

The sandstone petrology of the volcaniclastic turbidites of Unit A in the Lichi Mélange (<8.5–6.4 Ma) indicates a substantial component of arc-derived material. However, the εNd values ranging from −10.9 to −8.1 fall into the minor peaks of the Taiwan accretionary prism (Figure 16), indicating that the accretionary prism has contributed sediments to Unit A. Regional studies showed that the Tailuko belt in the eastern Central Range was not exhumed until ~2 Ma [*Dorsey*, 1988; *Huang et al.*, 2006; *Kirstein et al.*, 2010], and therefore, it could not have contributed sediments to the forearc basin until after this time. Hence, the εNd values of Unit A should reflect the mixing of volcanic clastics derived from the North Luzon Arc with syncollisional sediments derived from the Taiwan accretionary prism. The syncollisional sediments were likely concentrated in the finer portion of the volcaniclastic turbidites. The post 6.4 Ma forearc sediments (including Units B–D and the remnant forearc sequences) show a narrow, high peak, almost overlapping with the main peak of the accretionary prism (Figure 16). This observation indicates that the post 6.4 Ma forearc sediments were almost entirely derived from the accretionary prism, although some volcanic clastics still occur in Unit C.

It can be further inferred that during the deposition of Unit A in <8.5–6.4 Ma, both the volcanic arc and the accretionary prism were exposed above sea level. Given the small area of the volcanic islands of the present North Luzon Arc, this emergent accretionary prism might also have been very small. Thus, this period could be regarded as the incipient emergence of the accretionary prism. The considerable decrease of the εNd values since 6.4 Ma suggests that the arc-derived sediments were diluted rapidly by the massive amounts

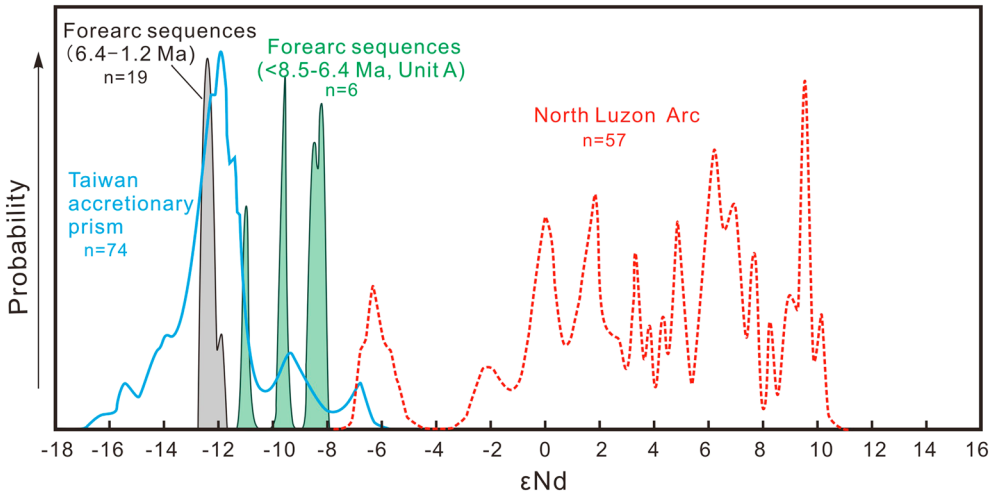

Figure 16. Relative probability plot of Nd isotopic compositional ranges of the <8.5–6.4 Ma and the 6.4–1.2 Ma forearc sediments. Also shown are those of the two possible sources: the Taiwan accretionary prism and the North Luzon Arc. Data of the Taiwan accretionary prism are compiled from the Central Range-Hsüehshan Range (Eocene to Miocene sediments and metasediments and pre-Cenozoic metamorphic basement) [*Chen et al.*, 1990b; *Lan et al.*, 2002] and the Hengchun Peninsula (Miocene sediments) [*Zhang et al.*, 2014]. Data of the North Luzon Arc are compiled from the Chimei-Chengkuangao volcanic islands on the Coastal Range and the Lutao-Lanyu volcanic islands offshore SE Taiwan [*Chen et al.*, 1990a; *Defant et al.*, 1990; *Lai et al.*, 2008, 2017; *Lai and Song*, 2013].

of prism-derived sediments and could hence be attributed to the growth and extensive exposure of the accretionary prism.

These inferences are also supported by the distribution of the benthic foraminifera in the Lichi Mélange (Figures 8 and 9). *Huang et al.* [2008] conducted a multivariate cluster analysis on the benthic foraminifera collected along the Mukeng-Chi section. Compared with our sampling sites, Unit A is dominated by indigenous deep water species without a significant occurrence of shallow-marine assemblages, indicating a locally exposed accretionary prism. However, Units B and C contain both indigenous deep water species and displaced shallow-water fauna, implying that the accretionary prism was extensively exposed, developing a shallow shelf. The shallow-marine benthic foraminifera in this shelf environment were then displaced into the deep forearc basin by turbidity currents.

7.3.2. Emergence of Taiwan Accretionary Prism

Based on the sedimentary record in the forearc sequences in the Lichi Mélange, the timing of the emergence of the Taiwan accretionary prism can be determined to lie within the interval of <8.5–6.4 Ma. This time interval is somewhat earlier than the age of the basal foreland surface in the western Taiwan (~6.5 Ma) [*Lin et al.*, 2003]. However, the ~6.5 Ma age was roughly estimated by the occurrence of *D. quinqueramus* (FAD: 8.12 Ma; LAD: 5.59 Ma) in the strata both below and above the surface and a K-Ar age determination (7.6–7.1 Ma) from a basalt layer ~25 m beneath the surface [*Lin et al.*, 2003; *Juang*, 1996]. Taking these data into account, the emergence of the Taiwan accretionary prism recorded in the forearc basin matches well with that recorded in the foreland basin (7.6–5.6 Ma). It is puzzling that a provenance shift from the volcanic arc to the accretionary prism was often observed at the base of the remnant forearc basin (~5.0 Ma according to the biostratigraphic framework of *Chi et al.* [1981]) in previous studies [*Teng*, 1979; *Dorsey*, 1988; *Huang et al.*, 2006]. This impression might be created by the contact relationship in which the remnant forearc sequences unconformably overlie the epiclastic rocks of the Tuluanshan Formation or by the temporary increase of volcanic detritus due to episodic volcanism.

As the emergence of the accretionary prism is one of the major features of the initial arc–continent collision [*Huang et al.*, 2000, 2006], the presence of the Taiwan-derived syncollisional sediments in the forearc basin provides a robust time constraint for the onset of collision within <8.5–6.4 Ma. This age is consistent with the older cooling events in the Central Range, i.e., the biotite Ar-Ar age of 7.9 ± 0.1 Ma [*Lo and Onstott*, 1995] and the zircon fission track age of 7.1 ± 1.3 Ma [*Mesalles et al.*, 2014]. Accepting that the Taiwan accretionary prism emerged at ~5 Ma, *Mesalles et al.* [2014], however, attributed these ages to cooling from below by the underthrusting plate. Based on our new stratigraphic results from the forearc basin, these ages might represent the earliest cooling event driven by the subaerial exhumation of the sedimentary cover of the

accretionary prism. The presence of the medium-grade metamorphic fragments and the totally reset zircon grains in the remnant forearc sequences since ~2 Ma [*Dorsey*, 1988; *Kirstein et al.*, 2010] might indicate a long period (<6.5–4.4 Myr) of erosion of the sedimentary cover. During the arc-continent collision in Timor, *Harris* [2011] proposed that the youngest passive margin sequences incorporated into the accretionary prism is an accurate determination of collision onset. The youngest known passive margin sequences incorporated into the Taiwan accretionary prism are the late Miocene turbidites exposed on the Hengchun Peninsula. They were roughly constrained within ~10.5–6.4 Ma (N15–17A) by the rare occurrence of planktonic foraminifera [*Chang*, 1964]. This age is consistent with our new stratigraphic results from the forearc basin. It also suggests that our study on the stratigraphy of the Lichi Mélange can provide a reliable age constraint on the Taiwan collision tectonics.

Recent studies have revealed that the growth of the Taiwan wedge during the arc-continent collision is essentially caused by structural underplating of material of the Chinese continental margin rather than by frontal accretion [e.g., *Beyssac et al.*, 2007; *Simoes et al.*, 2007]. Marine seismic reflection and wide-angle data acquired offshore southern Taiwan showed that a more than 200 km wide zone of extended to hyperextended continental crust of the Chinese continental margin is present south of the shelf, and it is subducting at the Manila Trench [*McIntosh et al.*, 2013; *Lester et al.*, 2013]. This thinned continental crust or transitional crust is then structurally underplated to the base of the accretionary prism. The studied sections are located just within the initial arc-continent collision zone defined by *Huang et al.* [2000], where the submarine Hengchun Ridge accretionary prism emerges as the Hengchun Peninsula. Therefore, the mechanism responsible for the initial emergence of the Taiwan accretionary prism within <8.5–6.4 Ma might also be underplating of the thinned continental crust.

7.4. Tectonic-Sedimentary Evolution of the Forearc Basin

By combining the sedimentary records extracted from the Lichi Mélange in this study with previous findings [*Chang et al.*, 2000, 2001; *Huang et al.*, 2008], we propose a model of the tectonic-sedimentary evolution of the forearc basin in the middle and southern Coastal Range as follows.

The eastward subduction of the South China Sea since 16 Ma gradually built the Taiwan accretionary prism and the North Luzon Arc. The forearc basin between the submarine accretionary prism and the volcanic arc was mainly floored by volcanic agglomerate and lacked terrestrial detritus (Figure 17a). By <8.5–6.4 Ma, the oceanic crust at the northern segment of the subduction zone had been totally eliminated, and the thinned continental crust was then underplated beneath the accretionary prism, leading to the emergence of the accretionary prism. The volcanic arc had also been exposed above sea level as isolated islands due to active volcanism. Sediments derived from these two tectono-morphographic units were thus shed into the forearc basin (Figure 17b). After ~6.4 Ma, the continuous underplating of the thinned continental crust contributed to the constant rising and extensive exposure of the accretionary prism, whose area was much larger than those of the volcanic islands. Therefore, the accretionary prism became the primary provenance of the forearc basin (Figure 17c). In response to the arc-continent collision, the sedimentation in the forearc basin was highly controlled by arcward back thrusting, and the western part was first deformed and uplifted (Figure 17c). As the back thrusting migrated eastward, the older forearc sequences (i.e., Units A–C) were entirely deformed and uplifted as a bathymetric high similar to the Huatung Ridge before 3.4 Ma. However, the remnant forearc basin in the east continued to receive synorogenic sediments until ~1.2 Ma (Figure 17d).

In the advanced arc-continent collision stage, the bathymetric high was further thrust westward and deformed into the Lichi Mélange (Figure 17d). Meanwhile, blocks of sedimentary rocks of the accretionary prism, basic and ultrabasic rocks of the volcanic arc-forearc basement, and andesitic rocks of the volcanic arc were emplaced into the Lichi Mélange [*Huang et al.*, 2008]. The lower parts of the remnant forearc sequences were also emplaced into the Lichi Mélange, forming Unit D (Figure 17d). The destruction of the forearc basin and the generation of the Lichi Mélange were accompanied by a series of deep tectonic events: the collision between the thick continental crust of the proximal margin and the North Luzon Arc [*Mesalles et al.*, 2014] and the deformation and even eastward subduction of the volcanic arc-forearc basement [*Hirtzel et al.*, 2009; *Tang and Chemenda*, 2000; *Chemenda et al.*, 2001; *Malavieille et al.*, 2002; *Malavieille and Trullenque*, 2009] (Figures 17d and 17e).

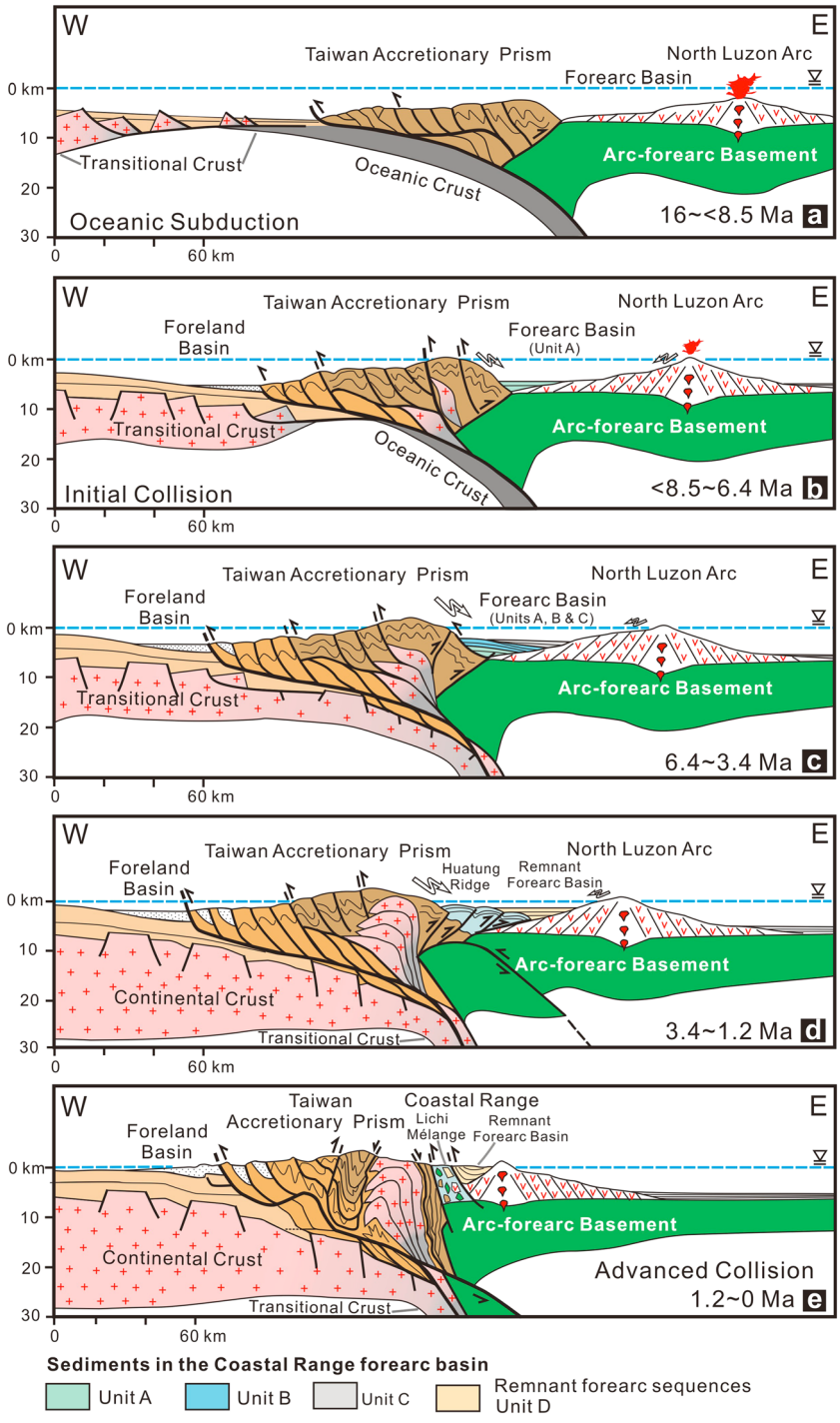

Figure 17. Tectonic-sedimentary evolution of the forearc basin in the middle and southern Coastal Range. The vertical exaggeration is approximately 2:1 and the fault angles have been adjusted accordingly. The internal structure of the subduction-collision system is primarily after the tectonic models published by *Malavieille et al.* [2002, 2016], *Malavieille and Trullenque* [2009], *McIntosh et al.* [2005, 2013], and *Lester et al.* [2013].

8. Conclusions

We successfully reconstruct the forearc basin sequences in the middle and southern Coastal Range from the tectonically disrupted Lichi Mélange and improve and expand the sedimentary records of the Taiwan arc-continent collision.

Detailed field investigations and biostratigraphic studies show that the lower parts of the forearc basin sequences are predominately preserved as the broken formation in the Lichi Mélange. The depositional ages of these forearc sequences range from the late Miocene to Pliocene (<8.5–3.0 Ma). They are obviously older than the normal sequences in the remnant forearc basin of 3.4–1.2 Ma in the east, demonstrating that the Lichi Mélange is not an olistostromal facies coeval with the remnant forearc sequence; rather, it originated from the shearing of the lower forearc sequences. The temporal-spatial variation of the forearc stratigraphy resembles the Huatung Ridge-remnant forearc basin in the North Luzon Trough off southeastern Taiwan and records the eastward back thrusting that occurred before 3.4 Ma during the arc-continent collision. The eastward back thrusting deformed and uplifted the older forearc strata (<8.5–3.4 Ma) as a bathymetric high similar to the Huatung Ridge in the west, while sedimentation in the remnant forearc basin in the east continued during 3.4–1.2 Ma. The vitrinite reflectance analysis shows that these older forearc strata did not experience significant burial and indicates that they were uplifted and exhumed shortly after deposition, which might have resulted from back thrusting. As the neodymium isotopic analysis shows, the oldest forearc sediments in the Lichi Mélange (<8.5–6.4 Ma) were derived from both the volcanic arc and the Taiwan accretionary prism. This finding indicates that the accretionary prism was exposed subaerially within <8.5–6.4 Ma, which provides a robust age constraint for the initiation of the arc-continent collision and might have resulted from the underplating by the thinned crust of the distal Chinese continental margin. As the accretionary prism was constantly rising and exposed over a large scale, forearc sediments younger than 6.4 Ma were mainly derived from the accretionary prism.

Acknowledgments

This work was financially cosupported by the National Natural Science Foundation of China (grants U1505231, 41472093, 91128211, 41476036, and 41606068) and the Knowledge Innovation Program of the Chinese Academy of Sciences (grant KZCX2-EW-101). This is contribution IS-2426 from GIGCAS. We thank Chih-Wei Chien for his help in the fieldwork and Yehua Shan and Hideki Mukoyoshi for their helpful discussions. Critical reviews and constructive comments by Ron Harris and an anonymous reviewer are greatly appreciated and have substantially improved the paper. All the data used in this paper are provided in the supporting information.

References

Anthonissen, D. E., and J. G. Ogg (2012), Appendix 3—Cenozoic and Cretaceous biochronology of planktonic foraminifera and calcareous nannofossils, in *The Geologic Time Scale 2012*, edited by F. M. Gradstein et al., pp. 1083–1127, Elsevier, Boston, Mass.

Barker, C. E. (1988), Geothermics of petroleum systems: Implication of the stabilization of kerogen thermal maturation after a geologically brief heating duration at peak temperature, *U.S. Geol. Surv. Bull.*, *1870*, 26–29.

Barker, C. E. (1989), Temperature and time in the thermal maturation of sedimentary organic matter, in *Thermal History of Sedimentary Basins*, edited by N. D. Naeser and T. H. McCulloh, pp. 73–98, Springer, New York.

Barrier, E., and C. Muller (1984), New observations and discussion on the origin and age of the Lichi Mélange, *Mem. Geol. Soc. China*, *6*, 303–325.

Beyssac, O., M. Simoes, J. P. Avouac, K. A. Farley, Y. G. Chen, Y. C. Chan, and B. Goffé (2007), Late Cenozoic metamorphic evolution and exhumation of Taiwan, *Tectonics*, *26*, TC6001, doi:10.1029/2006TC002064.

Blow, W. H. (1969), Late Middle Eocene to Recent planktonic foraminiferal biostratigraphy, in *Proceedings of the First International Conference on Planktonic Microfossils*, vol. 1, edited by P. Brönnimann and H. H. Renz, pp. 199–422 , E. J. Brill, Leiden.

Bown, P. R., and J. R. Young (1998), Techniques, in *Calcareous Nannofossil Biostratigraphy*, edited by P. R. Bown, pp. 16–28, Kluwer Acad., Dordrecht, Netherlands.

Cavazza, W., and M. Barone (2010), Large-scale sedimentary recycling of tectonic mélange in a forearc setting: The Ionian basin (Oligocene–Quaternary, southern Italy), *Geol. Soc. Am. Bull.*, *122*(11–12), 1932–1949.

Chang, C. P., J. Angelier, and C. Y. Huang (2000), Origin and evolution of a mélange: The active plate boundary and suture zone of the Longitudinal Valley, Taiwan, *Tectonophysics*, *325*, 43–62.

Chang, C. P., J. Angelier, C. Y. Huang, and C. S. Liu (2001), Structural evolution and significance of a mélange in a collision belt: The Lichi Mélange and the Taiwan arc-continent collision, *Geol. Mag.*, *138*(6), 633–651.

Chang, L. S. (1964), A biostratigraphic study of the Tertiary in the Hengchun Peninsula, Taiwan, based on smaller foraminifera (I: Northern Part), *Proc. Geol. Soc. China*, *7*, 48–62.

Chang, L. S. (1967), A biostratigraphic study of the Tertiary in the Coastal Range, eastern Taiwan, based on smaller foraminifera (I: Southern Part), *Proc. Geol. Soc. China*, *10*, 64–76.

Chang, L. S. (1968), A biostratigraphic study of the Tertiary in the Coastal Range, eastern Taiwan, based on smaller foraminifera (II. Northern Part), *Proc. Geol. Soc. China*, *11*, 19–33.

Chang, L. S. (1969), A biostratigraphic study of the Tertiary in the Coastal Range, eastern Taiwan, based on smaller foraminifera (III: Middle Part), *Proc. Geol. Soc. China*, *12*, 89–101.

Chang, L. S. (1972), Eocene/Miocene hiatus and N conglomerate in the Central Range of Taiwan, *Proc. Geol. Soc. China*, *15*, 93–98.

Chemenda, A. I., R. K. Yang, E. A. Konstantinovskaia, and G. M. Ivanov (2001), New results from physical modeling of arc-continent collision in Taiwan: Evolutionary model, *Tectonophysics*, *333*(1–2), 159–178.

Chen, C. H., Y. N. Shieh, T. Lee, C. H. Chen, and S. A. Mertzman (1990a), Nd-Sr-O isotopic evidence for source contamination and an unusual mantle component under Luzon Arc, *Geochim. Cosmochim. Acta*, *54*, 2473–2483.

Chen, C. H., B. M. Jahn, T. Lee, C. H. Chen, and J. Cornichet (1990b), Sm-Nd isotopic geochemistry of sediments from Taiwan and implications for the tectonic evolution of southeast China, *Chem. Geol.*, *88*(3), 317–332.

Chen, W. H., C. Y. Huang, Y. J. Lin, Q. Zhao, Y. Yan, D. Chen, X. Zhang, Q. Lan, and M. Yu (2015), Depleted deep South China Sea $\delta^{13}C$ paleoceanographic events in response to tectonic evolution in Taiwan–Luzon Strait since Middle Miocene, *Deep Sea Res. Part II*, *122*, 195–225, doi:10.1016/j.dsr2.2015.02.005.

Chi, W. C., and D. L. Reed (2008), Evolution of shallow, crustal thermal structure from subduction to collision: An example from Taiwan, *Geol. Soc. Am. Bull.*, *120*(5–6), 679–690.

Chi, W. C., L. Chen, C. S. Liu, and M. Brookfield (2014), Development of arc–continent collision mélanges: Linking onshore geological and offshore geophysical observations of the Pliocene Lichi Mélange, southern Taiwan and northern Luzon arc, western Pacific, *Tectonophysics*, *636*, 70–82.

Chi, W. R. (1982), The calcareous nannofossils of the Lichi mélange and the Kenting mélange and their significance in the interpretation of plate tectonics of the Taiwan region, *Ti-Chih*, *4*(1), 99–114.
Chi, W. R., J. Namson, and J. Suppe (1981), Stratigraphic record of plate interactions in the Coastal Range of eastern Taiwan, *Mem. Geol. Soc. China*, *4*, 155–194.
Chung, S. L., and S. S. Sun (1992), A new genetic model for the East Taiwan Ophiolite and its implications for Dupal domains in the Northern Hemisphere, *Earth Planet. Sci. Lett.*, *109*, 133–145.
Clift, P. D., H. Schouten, and A. E. Draut (2003), A general model of arc-continent collision and subduction polarity reversal from Taiwan and the Irish Caledonides, in *Intra-Oceanic Subduction Systems: Tectonic and Magmatic Processes*, edited by R. Larter and P. Leat, *Geol. Soc. London, Spec. Publ.*, *219*, 81–98.
Defant, M. J., R. Maury, J. L. Joron, M. D. Feigenson, J. Leterrier, H. Bellon, D. Jacques, and M. Richard (1990), The geochemistry and tectonic setting of the northern section of the Luzon arc (the Philippines and Taiwan), *Tectonophysics*, *183*(1), 187–205.
Dickinson, W. R. (1995), Forearc basins, in *Tectonics of Sedimentary Basins*, edited by C. J. Busby and R. V. Ingersoll, pp. 221–261, Blackwell Scientific, Cambridge.
Dorsey, R. J. (1988), Provenance evolution and unroofing history of a modern arc-continent collision: Evidence from petrography of Plio-Pleistocene sandstones, eastern Taiwan, *J. Sediment. Res.*, *58*(2), 208–218.
Dorsey, R. J., and N. Lundberg (1988), Lithofacies analysis and basin reconstruction of the Plio-Pleistocene collisional basin, Coastal Range of eastern Taiwan, *Acta Geol. Taiwan.*, *26*, 57–132.
Dorsey, R. J., E. J. Buchovecky, and N. Lundberg (1988), Clay mineralogy of Pliocene-Pleistocene mudstones, eastern Taiwan: Combined effects of burial diagenesis and provenance unroofing, *Geology*, *16*(10), 944–947.
Festa, A., Y. Dilek, G. A. Pini, G. Codegone, and K. Ogata (2012), Mechanisms and processes of stratal disruption and mixing in the development of mélanges and broken formations: Redefining and classifying mélanges, *Tectonophysics*, *568*, 7–24.
Gartner, S. (1990), Neogene calcareous nannofossil biostratigraphy, Leg 116 (Central Indian Ocean), in *Proc. ODP Sci. Results*, vol. 116, edited by J. R. Cochran and D. A. V. Stow, pp. 165–187, Ocean Drill. Program, College Station.
Goldstein, S. L., R. K. O'Nions, and P. J. Hamilton (1984), A Sm–Nd isotopic study of atmospheric dusts and particulates from river systems, *Earth Planet. Sci. Lett.*, *70*, 221–236.
Harris, R., J. Kaiser, A. Hurford, and A. Carter (2000), Thermal history of Australian passive margin cover sequences accreted to Timor during Late Neogene arc–continent collision, Indonesia, *J. Asian Earth Sci.*, *18*(1), 47–69.
Harris, R. A. (2011), The nature of the Banda Arc–continent collision in the Timor region, in *Arc-Continent Collision*, edited by D. Brown and P. D. Ryan, pp. 163–211, Springer, Berlin.
Harris, R. A., R. K. Sawyer, and M. G. Audley-Charles (1998), Collisional mélange development: Geologic associations of active mélange-forming processes with exhumed melange facies in the western Banda orogen, Indonesia, *Tectonics*, *17*, 458–480.
Hirtzel, J., W. C. Chi, D. Reed, L. Chen, C. S. Liu, and N. Lundberg (2009), Destruction of Luzon forearc basin from subduction to Taiwan arc-continent collision, *Tectonophysics*, *479*(1), 43–51.
Horng, C. S., and K. S. Shea (1996), Dating of the Plio-Pleistocene rapidly deposited sequence based on integrated magneto-biostratigraphy: A case study of the Madagida-chi Section, Coastal Range, eastern Taiwan, *J. Geol. Soc. China*, *39*, 31–58.
Hsü, K. J. (1968), Principles of mélanges and their bearing on the Franciscan-Knoxville Paradox, *Geol. Soc. Am. Bull.*, *79*, 1063–1074.
Hsu, T. L. (1956), Geology of the Coastal Range, eastern Taiwan, *Bull. Geol. Surv. Taiwan*, *8*, 39–64.
Hsu, T. L. (1976), The Lichi Mélange in the Coastal Range framework, *Bull. Geol. Surv. Taiwan*, *25*, 87–95.
Huang, C. Y., C. T. Shyu, S. B. Lin, T. Q. Lee, and D. D. Sheu (1992), Marine geology in the arc-continent collision zone off southeastern Taiwan: Implications for late Neogene evolution of the Coastal Range, *Mar. Geol.*, *107*, 183–212.
Huang, C. Y., P. B. Yuan, S. R. Song, C. W. Lin, C. Wang, M. T. Chen, C. T. Shyu, and B. Karp (1995), Tectonics of short-lived intra-arc basins in the arc-continent collision terrane of the Coastal Range, eastern Taiwan, *Tectonics*, *14*, 19–38, doi:10.1029/94TC02452.
Huang, C. Y., W. Y. Wu, C. P. Chang, S. Tsao, P. B. Yuan, C. W. Lin, and K. Y. Xia (1997), Tectonic evolution of accretionary prism in the arc-continent collision terrane of Taiwan, *Tectonophysics*, *281*, 31–51.
Huang, C. Y., P. B. Yuan, C. W. Lin, T. K. Wang, and C. P. Chang (2000), Geodynamic processes of Taiwan arc-continent collision and comparison with analogs in Timor, Papua New Guinea, Urals and Corsica, *Tectonophysics*, *325*, 1–21.
Huang, C. Y., P. B. Yuan, and S. J. Tsao (2006), Temporal and spatial records of active arc-continent collision in Taiwan: A synthesis, *Geol. Soc. Am. Bull.*, *118*(3–4), 274–288, doi:10.1130/B25527.1.
Huang, C. Y., C. W. Chien, B. Yao, and C. P. Chang (2008), The Lichi Mélange: A collision mélange formation along early arcward backthrusts during forearc basin closure, Taiwan arc-continent collision, *Geol. Soc. Am. Spec. Pap.*, *436*, 127–154, doi:10.1130/2008.2436(06).
Huang, T. Y. (1969), Some planktonic foraminiferous from a bore at Shihshan, near Taitung, Taiwan, *Proc. Geol. Soc. China*, *12*, 103–119.
Jahn, B. M. (1986), Mid-ocean ridge or marginal basin origin of the East Taiwan Ophiolite: Chemical and isotopic evidence, *Contrib. Mineral. Petrol.*, *92*, 194–206.
Jones, D. J. (1958), Displacement of microfossils, *J. Sediment. Res.*, *28*(4), 453–467.
Juang, W. S. (1996), Geochronology and geochemistry of basalts in the Western Foothills, Taiwan, *Bull. Natl. Museum Nat. Sci.*, *7*, 45–98.
Kelsey, H. M., B. L. Sherrod, R. J. Blakely, and R. A. Haugerud (2012), Holocene faulting in the Bellingham forearc basin: Upper-plate deformation at the northern end of the Cascadia subduction zone, *J. Geophys. Res.*, *117*, B03409, doi:10.1029/2011JB008816.
Kimbrough, D. L., D. P. Smith, J. B. Mahoney, T. E. Moore, M. Grove, R. G. Gastil, A. Ortega-Rivera, and C. M. Fanning (2001), Forearc-basin sedimentary response to rapid late cretaceous batholith emplacement in the Peninsular Ranges of southern and Baja California, *Geology*, *29*(6), 491–494.
Kirstein, L. A., M. G. Fellin, S. D. Willett, A. Carter, Y. G. Chen, J. I. Garver, and D. C. Lee (2010), Pliocene onset of rapid exhumation in Taiwan during arc–continent collision: New insights from detrital thermochronometry, *Basin Res.*, *22*(3), 270–285.
Lai, Y. M., and S. R. Song (2013), The volcanoes of an oceanic arc from origin to destruction: A case from the northern Luzon Arc, *J. Asian Earth Sci.*, *74*, 97–112, doi:10.1016/j.jseaes.2013.03.021.
Lai, Y. M., S. R. Song, and Y. Iizuka (2008), Magma mingling in the Tungho area, Coastal Range of eastern Taiwan, *J. Volcanol. Geotherm. Res.*, *178*, 608–623.
Lai, Y. M., S. R. Song, C. H. Lo, T. H. Lin, M. F. Chu, and S. L. Chung (2017), Age, geochemical and isotopic variations in volcanic rocks from the Coastal Range of Taiwan: Implications for magma generation in the Northern Luzon Arc, *Lithos*, *272*, 92–115.
Lan, C. Y., C. S. Lee, J. J. S. Shen, C. Y. Lu, S. A. Mertzman, and T. W. Wu (2002), Nd-Sr isotopic composition and geochemistry of sediments from Taiwan and their implications, *West Pacif. Earth Sci.*, *2*, 205–222.
Laughland, M. M., and M. B. Underwood (1993), Vitrinite reflectance and estimates of paleotemperature within the Upper Shimanto Group, Muroto Peninsula, Shikoku, Japan, *Mem. Geol. Soc. Am.*, *273*, 25–43.

Lee, Y. H., C. C. Chen, T. K. Liu, H. C. Ho, H. Y. Lu, and W. Lo (2006), Mountain building mechanisms in the Southern Central Range of the Taiwan Orogenic Belt—From accretionary wedge deformation to arc–continental collision, *Earth Planet. Sci. Lett.*, *252*(3), 413–422.
Lee, Y. H., T. Byrne, W. H. Wang, W. Lo, R. J. Rau, and H. Y. Lu (2015), Simultaneous mountain building in the Taiwan orogenic belt, *Geology*, *43*(5), 451–454.
Lester, R., K. McIntosh, H. J. Van Avendonk, L. Lavier, C. S. Liu, and T. K. Wang (2013), Crustal accretion in the Manila trench accretionary wedge at the transition from subduction to mountain-building in Taiwan, *Earth Planet. Sci. Lett.*, *375*, 430–440.
Liang, X. R., G. J. Wei, X. H. Li, and Y. Liu (2003), Precise measurement of 143Nd/144Nd and Sm/Nd ratios using multiple-collectors inductively coupled plasma-mass spectrometry (MC-ICPMS) [in Chinese with English abstract], *Geochimica*, *32*(1), 91–96.
Lin, A. T., A. B. Watts, and S. P. Hesselbo (2003), Cenozoic stratigraphy and subsidence history of the South China Sea margin in the Taiwan region, *Basin Res.*, *15*, 453–478, doi:10.1046/j.1365-2117.2003.00215.x.
Linn, A. M., D. J. DePaolo, and R. V. Ingersoll (1991), Nd-Sr isotopic provenance analysis of Upper Cretaceous Great Valley fore-arc sandstones, *Geology*, *19*(8), 803–806.
Liou, J. G., C. Y. Lan, J. Suppe, and W. G. Ernst (1977), The east Taiwan ophiolite: Its occurrence, petrology, metamorphism and tectonic setting, *Mining Res. Serv. Organ. Spec. Rep.*, *1*, 1–212.
Liu, T. K., S. Hsieh, Y. G. Chen, and W. S. Chen (2001), Thermo-kinematic evolution of the Taiwan oblique-collision mountain belt as revealed by zircon fission track dating, *Earth Planet. Sci. Lett.*, *186*(1), 45–56.
Lo, C. H., and T. C. Onstott (1995), Rejuvenation of K-Ar systems for minerals in the Taiwan Mountain Belt, *Earth Planet. Sci. Lett.*, *131*(1–2), 71–98.
Lo, C. H., T. C. Onstott, C. H. Chen, and T. Lee (1994), An assessment of $^{40}Ar/^{39}Ar$ dating for the whole-rock volcanic samples from the Luzon Arc near Taiwan, *Chem. Geol.*, *114*, 157–178.
Lundberg, N., D. L. Reed, C. S. Liu, and J. Lieske (1997), Forearc-basin closure and arc accretion in the submarine suture zone south of Taiwan, *Tectonophysics*, *274*(1), 5–23.
Malavieille, J., and G. Trullenque (2009), Consequences of continental subduction on forearc basin and accretionary wedge deformation in SE Taiwan: Insights from analogue modeling, *Tectonophysics*, *466*(3), 377–394.
Malavieille, J., S. E. Lallemand, S. Dominguez, A. Deschamps, C. Y. Lu, C. S. Liu, P. Schnürle, and the ACT Scientific Crew (2002), Arc-continent collision in Taiwan: New marine observations and tectonic evolution, *Geol. Soc. Am. Spec. Pap.*, *358*, 187–211.
Malavieille, J., G. Molli, M. Genti, S. Dominguez, O. Beyssac, A. Taboada, A. Vitale-Brovarone, C. Y. Lu, and C. T. Chen (2016), Formation of ophiolite-bearing tectono-sedimentary mélanges in accretionary wedges by gravity driven submarine erosion: Insights from analogue models and case studies, *J. Geodyn.*, *100*, 87–103.
Martini, E. (1971), Standard Tertiary and Quaternary calcareous nanoplankton zonation, in *Proceedings of the 2nd International Conference on Planktonic Microfossils*, vol. 2, edited by A. Farinacci, pp. 739–785, Tecnosci, Roma.
McCulloch, M. T., and G. J. Wasserburg (1978), Sm-Nd and Rb-Sr chronology of continental crust formation, *Science*, *200*(4345), 1003–1011.
McIntosh, K., Y. Nakamura, T. K. Wang, R. C. Shih, A. Chen, and C. S. Liu (2005), Crustal-scale seismic profiles across Taiwan and the western Philippine Sea, *Tectonophysics*, *401*(1), 23–54.
McIntosh, K., H. van Avendonk, L. Lavier, W. R. Lester, D. Eakin, F. Wu, C. S. Liu, and C. S. Lee (2013), Inversion of a hyper-extended rifted margin in the southern Central Range of Taiwan, *Geology*, *41*(8), 871–874.
Mesalles, L., F. Mouthereau, M. Bernet, C. P. Chang, A. T. S. Lin, C. Fillon, and X. Sengelen (2014), From submarine continental accretion to arc-continent orogenic evolution: The thermal record in southern Taiwan, *Geology*, *42*(10), 907–910.
Mitchell, C., S. A. Graham, and D. H. Suek (2010), Subduction complex uplift and exhumation and its influence on Maastrichtian forearc stratigraphy in the Great Valley Basin, northern San Joaquin Valley, California, *Geol. Soc. Am. Bull.*, *122*(11–12), 2063–2078.
Mukoyoshi, H., A. Sakaguchi, K. Otsuki, T. Hirono, and W. Soh (2006), Co-seismic frictional melting along an out-of-sequence thrust in the Shimanto accretionary complex. Implications on the tsunamigenic potential of splay faults in modern subduction zones, *Earth Planet. Sci. Lett.*, *245*(1), 330–343.
Ohmori, K., A. Taira, H. Tokuyama, A. Sakaguchi, M. Okamura, and A. Aihara (1997), Paleothermal structure of the Shimanto accretionary prism Shikoku, Japan: Role of an out-of- sequence thrust, *Geology*, *25*, 327–330.
Orange, D. L., and M. B. Underwood (1995), Patterns of thermal maturity as diagnostic criteria for interpretation of mélanges, *Geology*, *23*(12), 1144–1148.
Orme, D. A., B. Carrapa, and P. Kapp (2015), Sedimentology, provenance and geochronology of the upper Cretaceous–lower Eocene western Xigaze forearc basin, southern Tibet, *Basin Res.*, *27*(4), 387–411, doi:10.1111/bre.12080.
Page, B. M., and J. Suppe (1981), The Pliocene Lichi Mélange of Taiwan: Its plate tectonic and olistostromal origin, *Am. J. Sci.*, *281*, 193–227.
Paquet, F., J. N. Proust, P. M. Barnes, and J. R. Pettinga (2011), Controls on active forearc basin stratigraphy and sediment fluxes: The Pleistocene of Hawke Bay, New Zealand, *Geol. Soc. Am. Bull.*, *123*(5–6), 1074–1096.
Raymond, L. A. (1984), Classification of mélanges, *Geol. Soc. Am. Spec. Pap.*, *198*, 7–20.
Reed, D. L., N. Lundberg, C. S. Liu, and B. Y. Luo (1992), Structural relations along the margins of the offshore Taiwan accretionary wedge: Implications for accretion and crustal kinematics, *Acta Geol. Taiwan.*, *30*, 105–122.
Sakaguchi, A. (1999), Thermal maturity in the Shimanto accretionary prism, southwest Japan, with the thermal change of the subducting slab: Fluid inclusion and vitrinite reflectance study, *Earth Planet. Sci. Lett.*, *173*(1), 61–74.
Sakaguchi, A., A. Yanagihara, K. Ujiie, H. Tanaka, and M. Kameyama (2007), Thermal maturity of a fold–thrust belt based on vitrinite reflectance analysis in the Western Foothills complex, western Taiwan, *Tectonophysics*, *443*(3), 220–232.
Sekiguchi, K., and A. Hirai (1980), Estimation of maturation level of organic matter, *J. Jpn. Assoc. Pet. Technol.*, *45*, 39–47.
Shao, W. Y. (2015), Zircon U-Pb and Hf isotope constraints on the petrogenesis of igneous rocks in eastern Taiwan, PhD thesis, Natl. Taiwan Univ., Taipei, Taiwan.
Shyu, C. T., and S. C. Chen (1991), A topographic and magnetic analysis off southeastern Taiwan, *Acta Oceanogr. Taiwan*, *27*, 1–20.
Simoes, M., J. P. Avouac, O. Beyssac, B. Goffé, K. A. Farley, and Y. G. Chen (2007), Mountain building in Taiwan: A thermokinematic model, *J. Geophys. Res.*, *112*, B11405, doi:10.1029/2006JB004824.
Suppe, J. (1981), Mechanics of mountain building and metamorphism in Taiwan, *Mem. Geol. Soc. China*, *4*, 67–89.
Suppe, J. (1984), Kinematics of arc-continent collision, flipping of subduction, and back-arc spreading near Taiwan, *Mem. Geol. Soc. China*, *6*, 21–33.
Sweeney, J. J., and A. K. Burnham (1990), Evaluation of a simple model of vitrinite reflectance based on chemical kinetics (1), *AAPG Bull.*, *74*(10), 1559–1570.
Tang, J. C., and A. I. Chemenda (2000), Numerical modeling of arc-continent collision: Application to Taiwan, *Tectonophysics*, *325*, 23–42.
Teng, L. S. (1979), Petrographical study of the Neogene sandstones of the Coastal Range, eastern Taiwan (northern part), *Acta Geol. Taiwan.*, *20*, 129–156.

Teng, L. S. (1990), Geotectonic evolution of late Cenozoic arc-continent collision in Taiwan, *Tectonophysics*, *183*(1), 57–76.
Tsai, Y. B. (1986), Seismotectonics of Taiwan, *Tectonophysics*, *125*(1), 17–37.
Tissot, B. P., and D. H. Welte (1984), *Petroleum Formation and Occurrence*, Springer, New York.
Wade, B. S., P. N. Pearson, W. A. Berggren, and H. Pälike (2011), Review and revision of Cenozoic tropical planktonic foraminiferal biostratigraphy and calibration to the geomagnetic polarity and astronomical time scale, *Earth Sci. Rev.*, *104*(1), 111–142.
Wang, C. S. (1976), The Lichi Formation of the Coastal Range and arc-continent collision in eastern Taiwan, *Bull. Geol. Surv. Taiwan*, *25*, 73–86.
Williams, T. A., and S. A. Graham (2013), Controls on forearc basin architecture from seismic and sequence stratigraphy of the Upper Cretaceous Great Valley Group, central Sacramento Basin, California, *Int. Geol. Rev.*, *55*(16), 2030–2059.
Yamamoto, Y., H. Mukoyoshi, and Y. Ogawa (2005), Structural characteristics of shallowly buried accretionary prism: Rapidly uplifted Neogene accreted sediments on the Miura-Boso Peninsula, central Japan, *Tectonics*, *24*, TC5008, doi:10.1029/2005TC001823.
Yang, T. F., J. L. Tien, C. H. Chen, T. Lee, and R. S. Punongbayan (1995), Fission-track dating of volcanics in the northern part of the Taiwan-Luzon arc: Eruption ages and evidence for crustal contamination, *J. SE Asian Earth Sci.*, *11*(2), 81–93.
Yang, T. Y., T. K. Liu, and C. H. Chen (1988), Thermal event records of the Chimei igneoucomplex: Constraint on the ages of magma activities and structural implication based on fission track dating, *Acta Geol. Taiwan.*, *26*, 237–246.
Zhang, X., Y. Yan, C. Y. Huang, D. Chen, Y. Shan, Q. Lan, W. Chen, and M. Yu (2014), Provenance analysis and its geological significance to the Miocene accretionary prism of Hengchun Peninsula, southern Taiwan, *J. Asian Earth Sci.*, *85*, 26–39, doi:10.1016/j.jseaes.2014.01.021.
Zhang, X., P. A. Cawood, C. Y. Huang, Y. Wang, Y. Yan, M. Santosh, W. Chen, and M. Yu (2016), From convergent plate margin to arc–continent collision: Formation of the Kenting Mélange, Southern Taiwan, *Gondwana Res.*, *38*, 171–182, doi:10.1016/j.gr.2015.11.010.